ablated. In addition, a global approach for making a humanized mouse has been developed by transplanting human hepatocytes into the urokinase-type plasminogen activator(+/+)_severe-combined-immunodeficiency (*uPA/SCID*) mouse, which otherwise is immunodeficient and undergoes liver failure; these chimeric mice no longer develop liver failure, but rather the mouse liver comprises >70% human hepatocytes that propagate successfully and retain normal pharmacological functions such as drug metabolism (Tateno et al., 2004; Katoh et al., 2008). Eight human P450s (CYP1A2, 2A6, 2C8, 2C9, 2C19, 2D6, 3A4, 3A5), 35 other Phase I enzymes, and four classes of Phase II conjugating enzymes (UDP glucuronosyltransferases, glutathione *S*-transferases, *N*-acetyltransferases, and sulfotransferases) have been shown to be functional in chimeric mice (Katoh et al., 2008). Because each chimeric mouse will reflect the liver profile and genetic makeup of the human donor's hepatocytes, interindividual and ethnic differences in drug metabolism will undoubtedly exist. Nevertheless, variations of xenobiotic-metabolizing enzymes as well as other enzymes, receptors, transporters, transcription factors, and any other drug target located in human liver—might effectively be studied in such chimeric mouse lines.

Mammalian CYP1A1 basal mRNA is known to be negligible, resulting in no detectable CYP1A1 protein in any tissue, whereas basal levels of CYP1A2 mRNA and protein are relatively high in liver but generally low (protein undetectable on Western immunoblot) in nonhepatic tissues; induction by a CYP1 inducer such as chemicals in cigarette smoke or 2,3,7,8-tetrachlorodibenzo-*p*-dioxin (**TCDD**; **dioxin**) increases CYP1A1 and CYP1A2 mRNA and protein levels (Eaton et al., 1995; Nebert et al., 2004). Recently, two humanized *CYP1A1_1A2* lines were compared with C57BL/6J (**B6**) inbred mice with regard to expression of CYP1A1 and CYP1A2 mRNA levels following TCDD pretreatment. Maximally-induced mRNA concentrations of mouse CYP1A1 were ~10 times higher in liver and lung and ~100-fold greater in kidney than those of human CYP1A1 (Shi et al., 2008). On the other hand, maximally-induced mRNA levels of mouse CYP1A2 in liver were <2-fold higher than those of human CYP1A2. Maximally-induced mRNA levels of human CYP1A2 in liver were ~12 times higher than those of human CYP1A1, whereas maximally-induced mRNA levels of mouse CYP1A2 in liver were ~3-fold greater than those of mouse CYP1A1 (Shi et al., 2008).

These data caused us to query how "physiologically" relevant these human mRNA levels might be, in the intact mouse. Do these humanized mouse lines actually reflect "average" *CYP1A1* and *CYP1A2* gene expression that might be expected among individuals in a human population, or is this expression abnormally low or high? One should be able to shed some light on this, by comparing precise copy numbers of basal and TCDD-induced CYP1A1 and CYP1A2 mRNA (combined with quantification of protein levels and enzyme assays) in the humanized mouse lines versus wild-type mice.

Those who oppose the use of laboratory animals, and recommend instead that everyone utilize cells in culture, often declare that studies with cultured cell lines can provide information that would accurately reflect what is found in the intact animal. We therefore have compared the above-mentioned CYP1A1 and CYP1A2 parameters in liver from the humanized mouse lines and wild-type mice with those in human versus mouse hepatoma-derived established cell culture lines. The present study addresses these questions. Answering these questions should be beneficial, before launching into human risk assessment studies using such humanized mouse lines.

Material and methods

Mice. C57BL/6J (B6) mice were purchased from The Jackson Laboratory (Bar Harbor, ME). Development of the humanized *hCYP1A1_1A2_Cyp1a1/1a2(−/−)-Ahr^{b1}* transgenic line has been detailed (Dragin et al., 2007). Chimeric mice bearing human hepatocytes were generated using *uPA(+/+)/SCID* mice as the host (Giannini et al., 2003) and characterized (Tateno et al., 2004; Katoh et al., 2008); their human hepatocyte-replacement rates were between 73% and 83%. All experiments involving mice adhered to the Guidelines for Animal Experiments and Use Committee of the Nihon University School of Medicine.

Treatment of mice. Mice were treated with intraperitoneal TCDD (25 μg/kg for 24 h), versus corn oil vehicle alone for untreated. At least three groups ($N = 3$ each time) were studied to ensure reproducibility.

Cell cultures and treatment. The human HepG2 established cell line was derived from a hepatoblastoma (Dearfield et al., 1983). The mouse Hepa-1c1c7 line was derived from a C57L/J hepatoma (Bernhard et al., 1973). Cultured cells were treated with 10 nM TCDD for 24 h before total RNA isolation.

Reverse transcription. Total RNAs from samples were prepared by the acid guanidine thiocyanate-phenol/chloroform method (Tavangar et al., 1990). The cDNAs were synthesized using the ImProm-II Reverse Transcription system (Promega, Madison, WI) (Inaba et al., 2007).

Quantitative real-time PCR (qRT-PCR). We used the primers listed in Table 1. The qRT-PCR was performed in an ABI PRISM 7000 Sequence Detection System™ (Applied Biosystems), using Power SYBR Green PCR Master Mix (Applied Biosystems). Individual CYP1 mRNA abundance was determined, using the standard-curve method (from 10^1 to 10^8 copies/μL), as previously described by K. Livak (PE-ABI; Sequence Detector User; Bulletin #2) (Winer et al., 1999). Each sample was normalized to mouse glyceraldehyde-3-phosphate dehydrogenase (**GAPDH**) mRNA.

CYP1A mRNA copy numbers. Transcripts from the human *CYP1A1* and *CYP1A2* and the mouse *Cyp1a1* and *Cyp1a2* genes were quantified by fitting qRT-PCR data to a curve generated from cloned RNAs (cRNAs) for each CYP1. Briefly described, templates for cRNA synthesis were produced by PCR on cDNA constructs from each CYP1A cDNA that had been cloned into pcDNA3.1(+) (Invitrogen), using T7 RiboMAX™ Express Large-Scale RNA Production System (Promega) (Uno et al., 2006). The cRNAs were used to generate a standard curve in the PCR reactions from which mRNA copy numbers from qRT-RNA measurements could be extrapolated.

Western immunoblot analysis. Mice were euthanized by carbon dioxide asphyxiation followed by cervical dislocation. The liver was excised, and microsomes were prepared as previously described (Dalton et al., 2000). Protein concentrations were determined by the bicinchoninic acid method (Pierce Chemical Co.; Rockford, IL), according to details provided by the manufacturer. Microsomal proteins were separated on sodium dodecylsulfate (0.1%)–polyacrylamide (12%) minigels. Separated proteins were transferred to nitrocellulose membranes. Western immunoblot analysis was performed using goat polyclonal anti-rat CYP1A1/1A2 antibody; this antibody (Daiichi Pure Chemicals, Tokyo, Japan) recognizes both the human and mouse CYP1A1 and CYP1A2 proteins. We used alkaline phosphatase-conjugated secondary antibodies (Kirkegaard Perry Lab., Gaithersburg, MD) and the Alkaline

Table 1
Primer pairs used in qRT-PCR.

Gene	Forward primer	Reverse primer
hCYP1A1	5′-AAGGGGCGTTGTGTCTTTGT-3′	5′-ATACACTTCCGCTTGCCCAT-3′
hCYP1A2	5′-ACAAGGGACACAACGCTGAA-3′	5′-AGGGCTTGTTAATGGCAGTG-3′
mCyp1a1	5′-CCTCATGTACCTGGTAACCA-3′	5′-AAGGATGAATGCCGGAAGGT-3′
mCyp1a2	5′-AAGACAATGGCGGTCTCATC-3′	5′-GACGGTCAGAAAGCCGTGGT-3′
mGapdh	5′-TGCACCACCAACTGCTTAG-3′	5′-GATGCAGGGATGATGTTC-3′

h, human; m, mouse.

Phosphatase Conjugate Substrate Kit™ (Bio-Rad Lab., Hercules, CA), with exposure times ranging from 5 to 10 min.

Enzyme assays. Determination of microsomal BaP hydroxylase (Nebert and Gelboin, 1968) and ethoxyresorufin *O*-deethylase (**EROD**) (Burke et al., 1977) activities principally represent CYP1A1 activity. Acetanilide 4-hydroxylase (Shertzer et al., 2001) and methoxyresorufin *O*-demethylase (**MROD**) (Berthou et al., 1992; Hamm et al., 1998; Shertzer et al., 2001) activities principally (but not exclusively) represent CYP1A2 activity. These enzymes were assayed by the methods cited. Although the MROD spectrophotofluororometric assay is sensitive and reliable, it has been demonstrated (Hamm et al., 1998) that the MROD assay is not the most suitable for estimating CYP1A2 activity. In *Cyp1a2(−/−)* knockout mice, it was shown that hepatic MROD activity was increased 70-fold by TCDD treatment, indicating that other TCDD-inducible enzymes contribute to inducible MROD activity. In contrast, acetanilide 4-hydroxylase activity in *Cyp1a2(−/−)* knockout mice was induced only 2-fold by dioxin (Shertzer et al., 2001), suggesting that it is by far the preferred enzyme activity for estimating CYP1A2 catalytic expression.

Biohazard precaution. TCDD is highly toxic and regarded as a likely human carcinogen. All personnel were instructed in safe handling procedures. Lab coats, gloves and masks were worn at all times, and contaminated materials were collected separately for disposal by the Hazardous Waste Unit or by independent contractors. TCDD-treated mice were housed separately, and their carcasses regarded as contaminated biological materials. TCDD-treated cells in culture, and culture medium from these cells, were also regarded as contaminated biological materials.

Statistical analysis. Statistical significance between groups was determined by analysis-of-variance among groups and Student's *t*-test between groups. All assays were performed in duplicate or triplicate, and repeated at least twice. Statistical analyses were also carried out with the use of SAS® statistical software (SAS Institute Inc.; Cary, NC) and Sigma Plot (Systat Software, Inc., Point Richmond, CA).

Results and discussion

Factors affecting CYP expression

In a previous study of the entire gastrointestinal tract (Uno et al., 2008), large differences in basal but especially inducible CYP1A1 and CYP1A2 mRNA and protein levels were seen. This variability appears to depend on the route-of-administration and the target organ being studied: oral versus intraperitoneal administration of TCDD or BaP can drastically alter CYP1 mRNA levels in various cell types of the intestine, from tongue to colon (Uno et al., 2008). In two studies comparing humanized mice with wild-type controls (Dragin et al., 2007; Shi et al., 2008), large differences were also observed in human CYP1A1 or CYP1A2 mRNA, compared with mouse CYP1A1 or CYP1A2 mRNA. In the chimeric *uPA/SCID* humanized mouse, although CYP1A1 was not studied, large variability in CYP1A2 expression has also been seen (Katoh et al., 2008).

Reasons for differences in human transgene expression in humanized mouse tissues include: [a] genotype of the volunteer from whom the BAC library was derived (Jiang et al., 2005) or from whose hepatocytes were infused into a *uPA(+/+)/SCID* mouse (Katoh et al., 2008; [b] chromosomal location of the randomly inserted BAC transgene affecting transgene expression, *i.e.* the "neighborhood effect" (Bedell et al., 1996; Milot et al., 1996; Olson et al., 1996; Muller et al., 2001); [c] genetic background (modifier genes) of a particular inbred strain that can influence transgene expression (Bonyadi et al., 1997; Cranston and Fishel, 1999; Bennett et al., 2000); and [d] a BAC containing the human gene(s) (Jiang et al., 2005; Cheung et al., 2005) which does not include *trans*-regulatory, or all of the *cis*-regulatory, sites needed for "normal" expression of the transgene(s) in each mouse tissue or cell type studied.

Comparison of human versus mouse CYP1A1 mRNA levels in liver

Fig. 1A compares human and mouse CYP1A1 mRNA copy numbers in the *hCYP1A1_1A2_Cyp1a1/1a2(−/−)* line, B6 wild-type mice containing no human transgenes, chimeric *uPA/SCID* mice (**chimera**), and *uPA(+/+)/SCID* control mice containing no human hepatocytes (*uPA/SCID* mice). Human basal CYP1A1 mRNA levels in the liver of *hCYP1A1_1A2* and chimeric mice were quite low, having $\sim 1.3 \times 10^7$ and $\sim 1.2 \times 10^7$ transcript copy numbers (per μg total RNA), respectively; both were strikingly increased by TCDD to $\sim 7.3 \times 10^9$ and $\sim 2.0 \times 10^9$ copy numbers, respectively.

Mouse basal CYP1A1 mRNA levels in B6, chimeric, and *uPA/SCID* mice (Fig. 1A) were also quite low ($\sim 1.8 \times 10^6$, $\sim 1.7 \times 10^6$, and 1.0×10^6 copy numbers, respectively), but all were dramatically induced by TCDD to $\sim 2.5 \times 10^8$, $\sim 8.0 \times 10^7$, and $\sim 1.5 \times 10^8$ copy numbers, respectively. As expected, no human CYP1A1 mRNA was detected in B6 or *uPA/SCID* mice, and no mouse CYP1A1 mRNA was detected in the *hCYP1A1_1A2_Cyp1a1/1a2(−/−)* line.

Comparison of human versus mouse CYP1A2 mRNA levels in liver

Human basal CYP1A2 mRNA levels in *hCYP1A1_1A2_Cyp1a1/1a2(−/−)* and chimeric mice (Fig. 1B) were low ($\sim 2.6 \times 10^8$ and $\sim 0.89 \times 10^8$ transcript copy numbers, respectively). Both were significantly elevated by TCDD to $\sim 9.7 \times 10^8$ and $\sim 7.7 \times 10^8$ copy numbers, respectively.

Mouse basal CYP1A2 mRNA concentrations in B6, chimeric, and *uPA/SCID* mice were also low ($\sim 2.2 \times 10^8$, $\sim 0.16 \times 10^8$ and $\sim 1.2 \times 10^8$ copy numbers, respectively); all three were significantly induced by TCDD to $\sim 4.2 \times 10^9$, $\sim 0.73 \times 10^9$, and 2.8×10^9 copy numbers, respectively (Fig. 1B). As expected, no human CYP1A2 mRNA was detected in B6 and *uPA/SCID* mice, and no mouse CYP1A2 mRNA was detected in the *hCYP1A1_1A2_Cyp1a1/1a2(−/−)* line.

Comparison of human versus mouse CYP1A1 and CYP1A2 mRNA levels

It should be noted that the basal expression levels of human and mouse CYP1A2 mRNA ($1–3 \times 10^8$ copy numbers) were much higher (Fig. 1) than those of CYP1A1 mRNA ($\sim 10^7$ copy numbers). This conclusion supports the results of studies long ago (Nebert, 1989; Eaton et al., 1995). The induction of human and mouse CYP1A1 and CYP1A2 mRNAs by TCDD is also well known (Nebert, 1989; Eaton et al., 1995; Nebert et al., 2004).

A previous report (Shi et al., 2008) compared the expression of CYP1A1 and CYP1A2 mRNA in liver between two humanized *CYP1A1_1A2_Cyp1a1/1a2(−/−)* lines and the B6 inbred mouse: maximally-induced mRNA levels of mouse CYP1A1 were described as ~10 times higher than those of human CYP1A1; in contrast, maximally-induced mRNA levels of mouse CYP1A2 were <2-fold higher than those of human CYP1A2 in liver. However, the present study (in which we find a mouse/human induced CYP1A1 ratio of ~0.03 and a mouse/human induced CYP1A2 ratio of ~4) appears not to be consistent with this previous report.

The previous report also found that maximally-induced mRNA levels of human CYP1A2 in liver were ~12 times higher than those of human CYP1A1, whereas maximally-induced mRNA levels of mouse CYP1A2 were ~3-fold greater than those of mouse CYP1A1 (Shi et al., 2008). In the present study, these ratios are 0.13 and 16.8, respectively. These large differences in the calculated ratios clearly reflect the

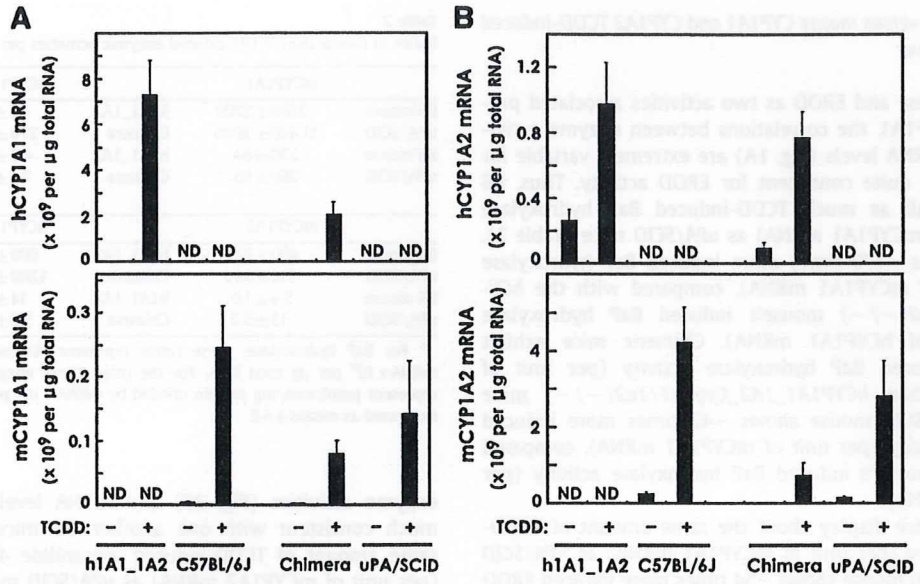

Fig. 1. Human (*upper panels*) versus mouse (*lower panels*) CYP1A1 (A) and CYP1A2 (B) mRNA copy numbers in liver from the *hCYP1A1_1A2_Cyp1a1/1a2(−/−)_Ahr*$^{h/-}$ mouse line, B6 inbred mouse, chimeric mouse, and *uPA/SCID* mouse—with, versus without, TCDD pretreatment. When administered, TCDD (25 μg/kg body weight 24 h before killing) was given intraperitoneally. "**ND**" (nondetectable by qRT-PCR) denotes nothing above background, whereas absence of "ND" (detectable, but extremely low by qRT-PCR) denotes something measurable above background. On *Y*-axis: **h**CYP1A1 or **h**CYP1A2 = human mRNA; **m**CYP1A1 or **m**CYP1A2 = mouse mRNA. For this figure and Fig. 4, the method for determining the copy number of mRNA molecules per μg total RNA is given in "Materials & methods". Note the different labels on the *Y*-axes of these figures. *Bars* and *brackets* denote means ± S.E.M., respectively ($N = 3$ independent experiments).

disparity between the "relative values" given in the previous report and the "absolute values" (*i.e.* copy numbers per μg total RNA) in the present study.

Human induced and basal CYP1A2 mRNA copy numbers in chimeric mice were 73–80% lower than those in *uPA/SCID* mice (Fig. 1B). This decrease can easily be explained when the human hepatocyte-replacement rate (73%–83%) is taken into account. This finding supports the notion that human hepatocytes in chimeric mice liver are affected by TCDD independently from mouse hepatocytes, suggesting that human hepatocytes in chimeric mice liver can mimic those in human liver.

The induction rate (Fig. 1) of human CYP1A1 mRNA in the *hCYP1A1_1A2_Cyp1a1/1a2(−/−)* line is quite remarkable (>500-fold), whereas that in chimeric mouse was not nearly as high (~170-fold). In contrast, the induction rate of human CYP1A2 mRNA in *hCYP1A1_1A2_Cyp1a1/1a2(−/−)* mice was ~3.7-fold, whereas that in the chimera was higher (~8.7-fold). These differences in fold-induction could be due to differences in the transcription regulatory regions associated with each of the two genes—if we assume that human and mouse genomic regulatory motifs might differ in their ability to govern these two human transgenes. This might not be a valid assumption, however, because many transcription factors and their DNA-binding motifs are highly conserved among vertebrates and, indeed, in some cases down to the fly, worm and yeast.

The BAC carrying the human *CYP1A1_CYP1A2* locus includes the 23.3-kb bidirectional promoter, plus 56 kb 3′-ward of *CYP1A1* and 86 kb 3′-ward of *CYP1A2* (Jiang et al., 2005). The transgenes in the *hCYP1A1_1A2_Cyp1a1/1a2(−/−)* mouse thus would carry human *cis*-regulatory motifs only within these sequences responsible for TCDD up-regulation, whereas expression of the human *CYP1A1* and *CYP1A2* genes in chimeric mice should be controlled by any and all of the human *cis*- and *trans*-regulatory enhancers in the same way as they are in human liver hepatocytes.

The expression level of mouse CYP1A1 induced mRNA in B6 is comparable to that in *uPA/SCID* mice and might also be comparable to that in chimeric mice when the human hepatocyte-replacement rate is taken into consideration. A similar conclusion might also be reached if one compares the expression levels of mouse induced CYP1A2 mRNA among B6, chimeric, and *uPA/SCID* mice. As a whole, we conclude that the *hCYP1A1_1A2_Cyp1a1/1a2(−/−)* line and the human hepatocyte chimeric mouse show similar expression levels of basal mRNA for the human *CYP1A1* and *CYP1A2* genes. Likewise, there are similar expression levels of TCDD-induced mRNA for these two genes, although their extent of induction is variable.

Comparison of human versus mouse CYP1A1 and CYP1A2 protein levels in liver

Western immunoblots of liver were carried out from the four mouse types, control versus TCDD-pretreated (Fig. 2). The polyvalent antiserum was raised against rat CYP1A1/1A2 and thus is not likely to recognize equally the human and mouse CYP1A1 and CYP1A2 proteins; consequently, a strict quantitative comparison of the human versus mouse orthologous protein concentrations is not possible. This problem has been recognized before and discussed in detail (Jiang et al., 2005).

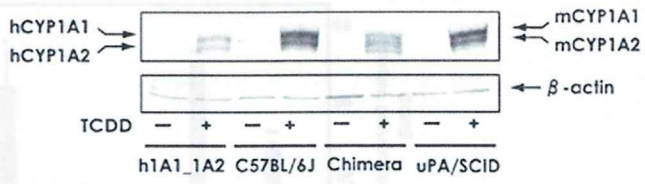

Fig. 2. Western immunoblot analysis of mouse versus human hepatic CYP1A1 and CYP1A2 proteins in the same mouse lines as in Fig. 1, using a polyclonal antibody that recognizes both mammalian CYP1A1 and CYP1A2. TCDD-induced mouse and human CYP1A1 proteins are both ~56.0 kDa, whereas TCDD-induced mouse and human CYP1A2 proteins are both ~54.5 kDa. Lanes 1–2 represent human CYP1A proteins only, whereas lanes 5–6 represent ~78% human CYP1A proteins and ~22% mouse CYP1A proteins. Lanes 3–4 and 7–8 depict only mouse CYP1A proteins. We used β-actin mRNA as a control for standardizing the amount of protein loaded per lane. The amount of microsomal protein (10 μg) loaded per lane was constant for all lanes.

Comparison of human versus mouse CYP1A1 and CYP1A2 TCDD-induced enzyme activities in liver

For BaP hydroxylase and EROD as two activities associated predominantly with CYP1A1, the correlations between enzyme activities (Fig. 3A) and mRNA levels (Fig. 1A) are extremely variable for BaP hydroxylase but quite consistent for EROD activity. Thus, B6 mice exhibit one-half as much TCDD-induced BaP hydroxylase activity (per unit of mCYP1A1 mRNA) as *uPA/SCID* mice (Table 2). The B6 mouse shows ~170 times more induced BaP hydroxylase activity (per unit of mCYP1A1 mRNA), compared with the *hCYP1A1_1A2_Cyp1a1/1a2(−/−)* mouse's induced BaP hydroxylase activity (per unit of hCYP1A1 mRNA). Chimeric mice exhibit ~6.2-fold more induced BaP hydroxylase activity (per unit of hCYP1A1 mRNA) than *hCYP1A1_1A2_Cyp1a1/1a2(−/−)* mice (Table 2). The *uPA/SCID* mouse shows ~42 times more induced BaP hydroxylase activity (per unit of mCYP1A1 mRNA), compared with the chimeric mouse's induced BaP hydroxylase activity (per unit of hCYP1A1 mRNA).

In contrast, B6 mice display about the same amount of TCDD-induced EROD activity (per unit of mCYP1A1 mRNA) as *uPA/SCID* mice (Table 2). The B6 mouse shows ~54 times more induced EROD activity (per unit of mCYP1A1 mRNA), compared with the *hCYP1A1_1A2_Cyp1a1/1a2(−/−)* mouse's induced EROD activity (per unit of hCYP1A1 mRNA). Chimeric mice exhibit ~1.7 times more induced EROD activity (per unit of hCYP1A1 mRNA) than *hCYP1A1_1A2_Cyp1a1/1a2(−/−)* mice (Table 2). The *uPA/SCID* mouse shows ~39 times more induced EROD activity (per unit of mCYP1A1 mRNA), compared with the chimeric mouse's induced EROD activity (per unit of hCYP1A1 mRNA).

Why does the humanized *hCYP1A1_1A2_Cyp1a1/1a2(−/−)* mouse carry so little enzyme activity toward BaP, compared with the chimeric mouse? This difference can be explained from the human hepatocyte-replacement rate (73%–83%) in chimeric mice. The liver of chimeric mice carries 73%–83% human hepatocytes, which exhibit extremely low BaP hydroxylase activity.

For acetanilide 4-hydroxylase and MROD as two activities associated predominantly with CYP1A2, the correlations between enzyme activities (Fig. 3B) and mRNA levels (Fig. 1B) are very much consistent with one another. B6 mice show virtually the same amount of TCDD-induced acetanilide 4-hydroxylase activity (per unit of mCYP1A2 mRNA) as *uPA/SCID* mice (Table 2). The B6 mouse shows about the same amount of induced acetanilide 4-hydroxylase activity (per unit of mCYP1A2 mRNA), compared with the *hCYP1A1_1A2_Cyp1a1/1a2(−/−)* mouse's induced acetanilide 4-hydroxylase activity (per unit of hCYP1A2 mRNA). Chimeric mice exhibit twice as much induced acetanilide 4-hydroxylase activity (per unit of hCYP1A2 mRNA) than *hCYP1A1_1A2_Cyp1a1/1a2(−/−)* mice (Table 2). The chimeric mouse shows ~2.3-fold more induced acetanilide 4-hydroxylase activity (per unit of mCYP1A2 mRNA), compared with the *uPA/SCID* mouse's induced acetanilide 4-hydroxylase activity (per unit of hCYP1A2 mRNA).

B6 mice exhibit one-half as much TCDD-induced MROD activity (per unit of mCYP1A2 mRNA) as *uPA/SCID* mice (Table 2). The *hCYP1A1_1A2_Cyp1a1/1a2(−/−)* mouse shows ~2-fold more induced MROD activity (per unit of mCYP1A2 mRNA), compared with the B6 mouse's induced MROD activity (per unit of hCYP1A2 mRNA). The *hCYP1A1_1A2_Cyp1a1/1a2(−/−)* mice exhibit ~2.4 times more in-

Table 2
Ratios of mouse liver TCDD-induced enzymic activities per unit of mRNA*.

	mCYP1A1		hCYP1A1	
B6 mouse	7600±2700	h1A1_1A2	44±13	BaP hydroxylase
uPA/SCID	11,400±3000	Chimera	270±62	
B6 mouse	230±64	h1A1_1A2	4.3±1.3	EROD activity
uPA/SCID	290±95	Chimera	7.4±3.1	
	mCYP1A2		**hCYP1A2**	
B6 mouse	490±84	h1A1_1A2	600±220	Acetanilide
uPA/SCID	510±200	Chimera	1200±390	4-hydroxylase
B6 mouse	5.4±1.0	h1A1_1A2	14±5.5	MROD activity
uPA/SCID	13±5.2	Chimera	5.6±0.3	

* For BaP hydroxylase, these ratios represent FU/min/mg protein divided by mRNA × 10^9 per μg total RNA. For the other three enzyme activities, these ratios represent pmol/min/mg protein divided by mRNA × 10^9 per μg total RNA. Values are expressed as means ± S.E.

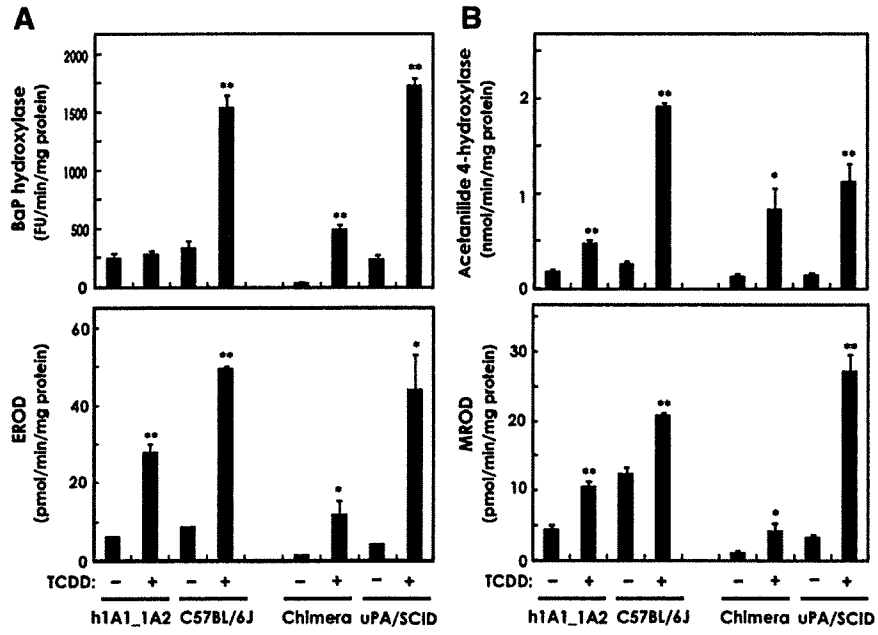

Fig. 3. (A) BaP hydroxylase and EROD activity (both representing largely CYP1A1), and (B) acetanilide 4-hydroxylase and MROD activity (both representing largely CYP1A2) in liver microsomes from the same mouse lines as in Fig. 1. FU, fluorescent units. *$P<0.05$ and **$P<0.01$, when comparing TCDD-pretreated with no pretreatment.

duced MROD activity (per unit of hCYP1A2 mRNA) than chimeric mice (Table 2). The *uPA/SCID* mouse shows twice as much induced MROD activity (per unit of mCYP1A2 mRNA), compared with the chimeric mouse's induced MROD activity (per unit of hCYP1A2 mRNA). Expression of CYP1A2 catalytic activity, relative to CYP1A2 mRNA levels, in the humanized *hCYP1A1_1A2_Cyp1a1/1a2(−/−)* and chimeric mouse lines is therefore very robust and within 2-fold similar to that expressed in mouse liver.

Comparison of human versus mouse CYP1A1 and CYP1A2 mRNA levels in hepatoma-derived cell culture lines

Animal rights' activists have urged scientists to study physiological functions in cell cultures rather than using live laboratory animals. Many studies have shown, however, that parameters found in cell culture do not accurately reflect what happens in the intact animal.

How does the expression of the *CYP1A1* and *CYP1A2* genes in intact liver compare with that in hepatoma-derived established cell lines? In HepG2 cells (Fig. 4A), human basal CYP1A1 mRNA was negligible, whereas human TCDD-induced CYP1A1 mRNA gave ~5.4×10^{9} copy numbers (per μg total RNA). In Hepa-1c1c7 cells (Fig. 4A), mouse basal versus TCDD-induced CYP1A1 mRNA showed ~0.35×10^{8} and ~1.9×10^{8} copy numbers, respectively. Mouse CYP1A1 mRNA was not detected in HepG2, and human CYP1A1 mRNA was not detected in Hepa-1c1c7 cells.

In HepG2 cells (Fig. 4B), human basal versus TCDD-induced CYP1A2 mRNA gave ~0.27×10^{6} and ~4.8×10^{6} copy numbers, respectively. In Hepa-1c1c7 cells (Fig. 4B), mouse basal versus TCDD-induced CYP1A2 mRNA showed ~0.14×10^{6} and ~1.2×10^{6} copies, respectively. Mouse CYP1A2 mRNA was not detected in HepG2, and human CYP1A2 mRNA was not detected in Hepa-1c1c7 cells.

Thus, in livers of the *hCYP1A1_1A2_Cyp1a1/1a2(−/−)* and chimeric mice, the copy number of human induced CYP1A1 mRNA is 7.5 and 2.6 times, respectively, greater than that of human induced CYP1A2 mRNA. On the other hand, in the HepG2 liver-derived established cell line, the copy number of human induced CYP1A1 mRNA is more than 1100 times greater than that of human induced CYP1A2 mRNA. In livers of the B6 and *uPA/SCID* mice, the copy number of mouse induced CYP1A2 mRNA is 40-fold and 20-fold, respectively, greater than that of mouse induced CYP1A1 mRNA; in contrast, in the Hepa-1c1c7 established cell line, the copy number of mouse induced CYP1A1 mRNA is almost 1600-fold greater than that of mouse maximally-inducible CYP1A2 mRNA. This decline in *CYP1A2* gene expression seen in established cell lines reflects the well-known fact that numerous "housekeeping" genes such as *CYP1A2* are extinguished, or are greatly decreased in expression—in tumor cells as well as "established", or transformed, cell lines in culture (Owens et al., 1975; Nebert, 2006). However, such suppression often does not occur for the *CYP1A1* gene in differentiated tumors, including the HepG2 and Hepa-1c1c7 hepatoma-derived cell lines (Owens et al., 1975; Nebert, 2006).

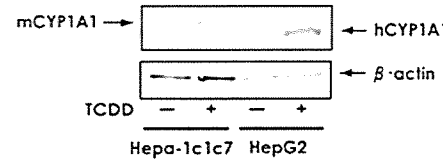

Fig. 5. Western immunoblot analysis of mouse versus human hepatic CYP1A1 and CYP1A2 proteins in the same cell culture lines as in Fig. 4. Everything is the same as that described for the Western blot in Fig. 2. The amount of cell culture protein (10 μg) loaded per lane was constant for all lanes.

Comparison of human versus mouse CYP1A1 and CYP1A2 protein levels in hepatoma-derived cell culture lines

We carried out Western immunoblots of Hepa-1c1c7 and HepG2 cells, control versus TCDD-pretreated (Fig. 5). The human CYP1A1 protein appears to migrate more rapidly than the mouse CYP1A1 protein. We believe the level of CYP1A2 protein was so low that it was not detected in either established hepatoma cell line.

Comparison of human versus mouse CYP1A1 and CYP1A2 TCDD-induced enzyme activities in hepatoma-derived cell culture lines

Different from what was found in mouse liver, the correlations between enzyme activities (Fig. 6A) and mRNA levels (Fig. 4A) are extremely variable for EROD activity but more consistent for BaP

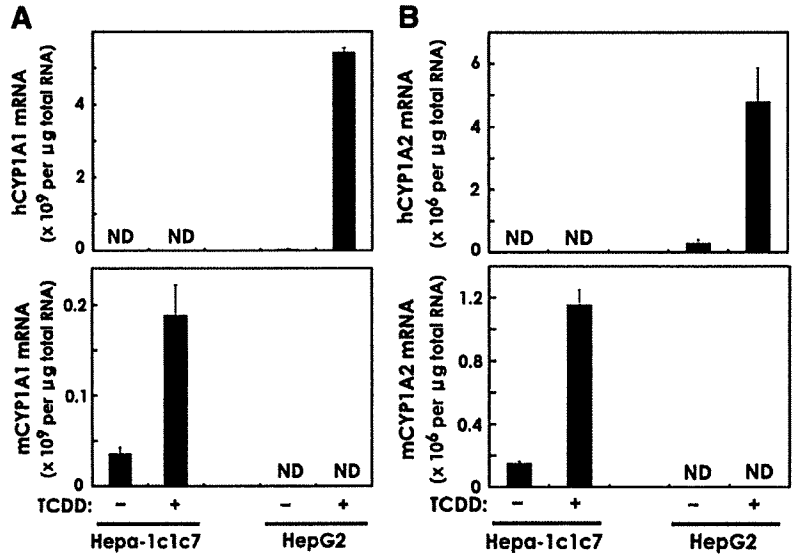

Fig. 4. Human (*upper panels*) versus mouse (*lower panels*) CYP1A1 (A) and CYP1A2 (B) mRNA copy numbers in mouse Hepa-1c1c7 cells and human HepG2 cells—with, versus without, TCDD exposure (10 nM for 24 h) in culture. Abbreviations are the same as those in Fig. 1.

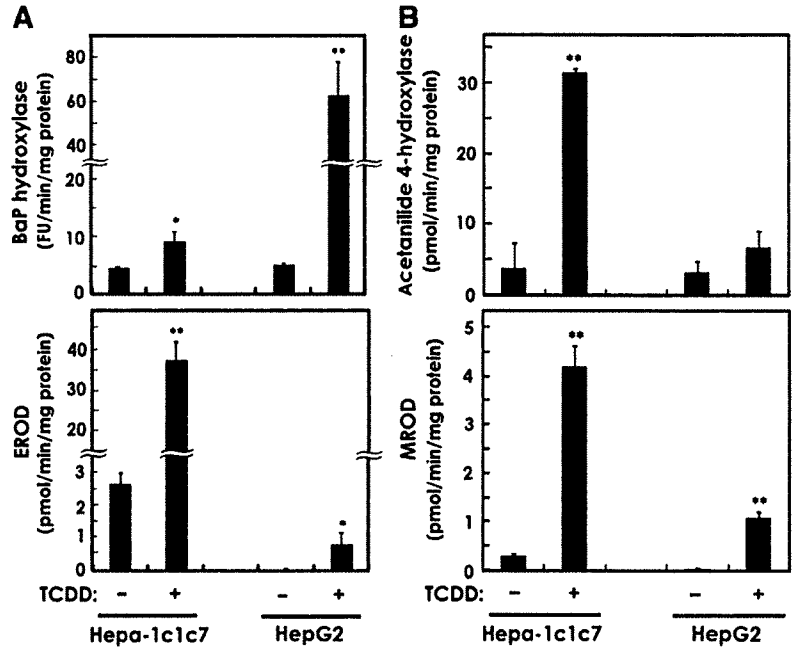

Fig. 6. (A) BaP hydroxylase and EROD activity (both representing largely CYP1A1), and (B) acetanilide 4-hydroxylase and MROD activity (both representing largely CYP1A2) in the same cell culture lines as in Fig. 4. $^{*}P<0.05$ and $^{**}P<0.01$, when comparing TCDD-pretreated with no pretreatment.

hydroxylase activity. Hepa-1c1c7 cells show ~4.8 times more TCDD-induced BaP hydroxylase activity (per unit of mCYP1A1 mRNA) than HepG2 cells exhibit for induced BaP hydroxylase activity (per unit of hCYP1A1 mRNA) (Table 3). Hepa-1c1c7 cells show ~1500 times more TCDD-induced EROD activity (per unit of mCYP1A1 mRNA) than HepG2 cells exhibit for induced EROD activity (per unit of hCYP1A1 mRNA). For whatever reason, HepG2 cells do not display very high induced BaP hydroxylase activity, and their induced EROD activity is extremely low.

For acetanilide 4-hydroxylase and MROD as two activities associated predominantly with CYP1A2, the correlations between enzyme activities (Fig. 6B) and mRNA levels (Fig. 6B) are better than those with CYP1A1. Hepa-1c1c7 cells show ~16-fold more TCDD-induced acetanilide 4-hydroxylase activity (per unit of mCYP1A2 mRNA) than HepG2 cells exhibit for induced acetanilide 4-hydroxylase activity (per unit of hCYP1A2 mRNA) (Table 3). Hepa-1c1c7 cells show ~15-fold more TCDD-induced MROD activity (per unit of mCYP1A2 mRNA) than HepG2 cells exhibit for induced MROD activity (per unit of hCYP1A2 mRNA). Therefore, HepG2 cells do not express either CYP1A1 or CYP1A2 activities nearly as robustly as do Hepa-1c1c7 cells.

Table 3
Ratios of hepatoma-derived cell line TCDD-induced enzymic activities per unit of mRNA*.

	mCYP1A1		hCYP1A1	
Hepa-1c1c7	55±21	HepG2	11±2.5	BaP hydroxylase
Hepa-1c1c7	210±48	HepG2	0.14±0.06	EROD activity
	mCYP1A2		**hCYP1A2**	
Hepa-1c1c7	27,000±2400	HepG2	1800±930	Acetanilide 4-hydroxylase
Hepa-1c1c7	3700±480	HepG2	250±85	MROD activity

* For BaP hydroxylase, these ratios represent FU/min/mg protein divided by mRNA × 10^9 per μg total RNA. For the other three enzyme activities, these ratios represent pmol/min/mg protein divided by mRNA × 10^9 per μg total RNA. Values are expressed as means ± S.E.

Conclusions

In this study we have measured the amount of variability between human and mouse CYP1A mRNA and protein levels and corresponding enzyme activities in the humanized *hCYP1A1_1A2_Cyp1a1/1a2(−/−)* and chimeric *uPA/SCID* lines, by comparing these parameters with those seen in wild-type mice from which these two lines were derived. We have also compared these mRNA and protein levels and corresponding enzyme activities in mouse hepatoma-derived Hepa-1c1c7 and human hepatoblastoma-derived HepG2 established cell culture lines. Clearly, the CYP1A1/CYP1A2 activity ratios in these hepatoma-derived established cell lines are not accurate indicators of those in liver from the intact mouse. Undoubtedly, this discrepancy is primarily caused by the dramatically lowered CYP1A2 mRNA levels—presumably due to "extinction" of the normal expression of the *CYP1A2* gene in these hepatoma-derived established cell lines. Not only very low CYP1A2 enzyme activity per unit of mRNA was seen in both Hepa-1c1c7 and HepG2 cells, but also low CYP1A1 enzyme activity per unit of hCYP1A1 mRNA was found in HepG2 cells.

Comparing liver of the two humanized mouse lines with liver of mice from which these two humanized lines were derived was most disturbing when one examined CYP1A1-specific (BaP and ethoxyresorufin) and CYP1A2-specific (acetanilide and methoxyresorufin) substrates metabolized—per unit of mCYP1A1, hCYP1A1, mCYP1A2 or hCYP1A2 mRNA. The hCYP1A1 in mouse liver was between 38 and more than 170 times less efficient than mCYP1A1 in the hydroxylation of BaP and about 54-fold less efficient in EROD activity. In contrast, hCYP1A2 in mouse liver appeared to function nearly equivalent to mCYP1A2 in wild-type mouse liver.

The levels of human CYP1A1 and CYP1A2 mRNA in both humanized mouse lines appear to be quite compatible with what might be expected among individual persons in any human population. It is very clear, however, that substrate specificity varies widely, independent of human versus mouse CYP1A1/1A2 mRNA or protein concentrations. Nevertheless, keeping this caveats in mind, both of these lines should still be useful for studies in human risk assessment, toxicology, pharmacology, and other medical subspecialties.

Note added in proof

A recent study (Wilson et al., 2008) is directly relevant to the problems addressed in our present manuscript. This study involves Tc1 hepatocytes, derived from an aneuploid mouse strain carrying human chromosome (Chr) 21 in addition to the entire mouse genome. The authors compared the regulation of human genes in Tc1 cells to that of the mouse orthologous genes in these same cells, using mouse wild-type versus human wild-type cells as controls. Regulation in the nuclei of Tc1 cells was compared at three levels: binding of transcription factors to DNA, modification of histones, and gene expression. The binding patterns of HNF1α, HNF4α and HNF6 on human Chr 21 in Tc1 cells matched closely those seen in human wild-type cells, rather than those seen in mouse wild-type cells. Similarly, histone modifications–as well as gene expression (the amount of mRNA transcribed)–showed human-specific, instead of mouse-specific, patterns on human Chr 21 in Tc1 cells. The authors concluded that it is the regulatory DNA sequence, rather than any other species-specific factor, which is the single most important determinant of gene expression (Wilson et al., 2008).

Acknowledgments

We thank our colleagues for many fruitful discussions and careful readings of this manuscript. Supported, in part, by the Ministry of Education, Science, Sports & Culture, Japan (Grant-in-Aid for Scientific Research on Priority Areas, 18077005 to S.U. and M.M.), and Nihon University Joint Research Grant for 2007 (S.U.), and NIH Grants R01 ES014403 (D.W.N.) and P30 ES06096 (D.W.N.).

References

Aoyama, T., Gonzalez, F.J., Gelboin, H.V., 1989. Human cDNA-expressed cytochrome P450 1A2: mutagen activation and substrate specificity. Mol. Carcinog. 2, 192–198.
Bedell, M.A., Jenkins, N.A., Copeland, N.G., 1996. Good genes in bad neighbourhoods. Nat. Genet. 12, 229–232.
Bennett, L.M., McAllister, K.A., Blackshear, P.E., Malphurs, J., Goulding, G., Collins, N.K., Ward, T., Bunch, D.O., Eddy, E.M., Davis, B.J., Wiseman, R.W., 2000. *Brca2*-null embryonic survival is prolonged on the BALB/c genetic background. Mol. Carcinog. 28, 174–183.
Bernhard, H.P., Darlington, G.J., Ruddle, F.H., 1973. Expression of liver phenotypes in cultured mouse hepatoma cells: synthesis and secretion of serum albumin. Dev. Biol. 35, 83–96.
Berthou, F., Guillois, B., Riche, C., Dreano, Y., Jacqz-Aigrain, E., Beaune, P.H., 1992. Interspecies variations in caffeine metabolism related to cytochrome P450 1A enzymes. Xenobiotica 22, 671–680.
Bonyadi, M., Rusholme, S.A., Cousins, F.M., Su, H.C., Biron, C.A., Farrall, M., Akhurst, R.J., 1997. Mapping of a major genetic modifier of embryonic lethality in *Tgfb1(−/−)* knockout mice. Nat. Genet. 15, 207–211.
Burke, M.D., Mayer, R.T., Kouri, R.E., 1977. 3-Methylcholanthrene-induced monooxygenase (*O*-deethylation) activity of human lymphocytes. Cancer Res. 37, 460–463.
Cheung, C., Ma, X., Krausz, K.W., Kimura, S., Feigenbaum, L., Dalton, T.P., Nebert, D.W., Idle, J.R., Gonzalez, F.J., 2005. Differential metabolism of 2-amino-1-methyl-6-phenylimidazo[4,5-*b*]pyridine (PhIP) in mice humanized for CYP1A1 and CYP1A2. Chem. Res. Toxicol. 18, 1471–1478.
Cranston, A., Fishel, R., 1999. Female embryonic lethality in *Msh2–Trp53* nullizygous mice is strain-dependent. Mamm. Genome 10, 1020–1022.
Dalton, T.P., Dieter, M.Z., Matlib, R.S., Childs, N.L., Shertzer, H.G., Genter, M.B., Nebert, D.W., 2000. Targeted knockout of *Cyp1a1* gene does not alter hepatic constitutive expression of other genes in the mouse [*Ah*] battery. Biochem. Biophys. Res. Commun. 267, 184–189.
Dearfield, K.L., Jacobson-Kram, D., Brown, N.A., Williams, J.R., 1983. Evaluation of a human hepatoma cell line as a target cell in genetic toxicology. Mutat. Res. 108, 437–449.
Derkenne, S., Curran, C.P., Shertzer, H.G., Dalton, T.P., Dragin, N., Nebert, D.W., 2005. Theophylline pharmacokinetics: comparison of *Cyp1a1(−/−)* and *Cyp1a2(−/−)* knockout mice, humanized *hCYP1A1_1A2* knock-in mice lacking either the mouse *Cyp1a1* or *Cyp1a2* gene, and *Cyp1(+/+)* wild-type mice. Pharmacogenet. Genomics 15, 503–511.
Dragin, N., Uno, S., Wang, B., Dalton, T.P., Nebert, D.W., 2007. Generation of 'humanized' *hCYP1A1_1A2_Cyp1a1/1a2(−/−)* mouse line. Biochem. Biophys. Res. Commun. 359, 635–642.
Eaton, D.L., Gallagher, E.P., Bammler, T.K., Kunze, K.L., 1995. Role of cytochrome P450 1A2 in chemical carcinogenesis: implications for human variability in expression and enzyme activity. Pharmacogenetics 5, 259–274.
Giannini, C., Morosan, S., Tralhao, J.G., Guidotti, J.E., Battaglia, S., Mollier, K., Hannoun, L., Kremsdorf, D., Gilgenkrantz, H., Charneau, P., 2003. A highly efficient, stable, and rapid approach for ex vivo human liver gene therapy via a FLAP lentiviral vector. Hepatology 38, 114–122.
Hamm, J.T., Ross, D.G., Richardson, V.M., Diliberto, J.J., Birnbaum, L.S., 1998. Methoxyresorufin: an inappropriate substrate for CYP1A2 in the mouse. Biochem. Pharmacol. 56, 1657–1660.
Inaba, Y., Yamamoto, K., Yoshimoto, N., Matsunawa, M., Uno, S., Yamada, S., Makishima, M., 2007. Vitamin D3 derivatives with adamantane or lactone ring side chains are cell type-selective vitamin D receptor modulators. Mol. Pharmacol. 71, 1298–1311.
Jiang, Z., Dalton, T.P., Jin, L., Wang, B., Tsuneoka, Y., Shertzer, H.G., Deka, R., Nebert, D.W., 2005. Toward the evaluation of function in genetic variability: characterizing human SNP frequencies and establishing BAC-transgenic mice carrying the human *CYP1A1_CYP1A2* locus. Hum. Mutat. 25, 196–206.
Katoh, M., Tateno, C., Yoshizato, K., Yokoi, T., 2008. Chimeric mice with humanized liver. Toxicology 246, 9–17.
Lindberg, R.L., Negishi, M., 1989. Alteration of mouse cytochrome P450coh substrate specificity by mutation of a single amino-acid residue. Nature 339, 632–634.
Milot, E., Fraser, P., Grosveld, F., 1996. Position effects and genetic disease. Trends Genet. 12, 123–126.
Muller, K., Heller, H., Doerfler, W., 2001. Foreign DNA integration. Genome-wide perturbations of methylation and transcription in the recipient genomes. J. Biol. Chem. 276, 14271–14278.
Nebert, D.W., 1989. The *Ah* locus: genetic differences in toxicity, cancer, mutation, and birth defects. Crit. Rev. Toxicol. 20, 153–174.
Nebert, D.W., 2006. Comparison of gene expression in cell culture to that in the intact animal: relevance to drugs and environmental toxicants. Am. J. Physiol., Cell Physiol. 290, C37–C41.
Nebert, D.W., Dalton, T.P., 2006. The role of cytochrome P450 enzymes in endogenous signalling pathways and environmental carcinogenesis. Nat. Rev., Cancer 6, 947–960.
Nebert, D.W., Gelboin, H.V., 1968. Substrate-inducible microsomal aryl hydroxylase in mammalian cell culture. I. Assay and properties of induced enzyme. J. Biol. Chem. 243, 6242–6249.
Nebert, D.W., Dalton, T.P., Okey, A.B., Gonzalez, F.J., 2004. Role of aryl hydrocarbon receptor-mediated induction of the CYP1 enzymes in environmental toxicity and cancer. J. Biol. Chem. 279, 23847–23850.
Nelson, D.R., Koymans, L., Kamataki, T., Stegeman, J.J., Feyereisen, R., Waxman, D.J., Waterman, M.R., Gotoh, O., Coon, M.J., Estabrook, R.W., Gunsalus, I.C., Nebert, D.W., 1996. P450 superfamily: update on new sequences, gene mapping, accession numbers and nomenclature. Pharmacogenetics 6, 1–42.
Nelson, D.R., Zeldin, D.C., Hoffman, S.M., Maltais, L.J., Wain, H.M., Nebert, D.W., 2004. Comparison of cytochrome P450 (*CYP*) genes from the mouse and human genomes, including nomenclature recommendations for genes, pseudogenes, and alternative-splice variants. Pharmacogenetics 14, 1–18.
Nichols, R.C., Cooper, S., Trask, H.W., Gorman, N., Dalton, T.P., Nebert, D.W., Sinclair, J.F., Sinclair, P.R., 2003. Uroporphyrin accumulation in hepatoma cells expressing human or mouse CYP1A2: relation to the role of CYP1A2 in human porphyria cutanea tarda. Biochem. Pharmacol. 65, 545–550.
Olson, E.N., Arnold, H.H., Rigby, P.W., Wold, B.J., 1996. Know your neighbors: three phenotypes in null mutants of the myogenic bHLH gene *Mrf4*. Cell 85, 1–4.
Owens, I.S., Niwa, A., Nebert, D.W., 1975. In: Gerschenson, L.E., Thompson, E.B. (Eds.), Expression of Aryl Hydrocarbon Hydroxylase Induction in Liver- and Hepatoma-Derived Cell Cultures. Academic Press, New York, NY, pp. 378–401.
Shertzer, H.G., Nebert, D.W., Senft, A.P., Dingledein, M., Genter, M.B., Dalton, T.P., 2001. Spectrophotometric assay for acetanilide 4-hydroxylase, an estimate of CYP1A2 enzyme activity. Toxicol. Meth. 11, 81–88.
Shi, Z., Chen, Y., Dong, H., Amos-Kroohs, R.M., Nebert, D.W., 2008. Generation of 'humanized' *hCYP1A1_1A2_Cyp1a1/1a2(−/−)_Ahr*^{d} mouse line harboring the poor-affinity aryl hydrocarbon receptor. Biochem. Biophys. Res. Commun. 376, 775–780.
Tateno, C., Yoshizane, Y., Saito, N., Kataoka, M., Utoh, R., Yamasaki, C., Tachibana, A., Soeno, Y., Asahina, K., Hino, H., Asahara, T., Yokoi, T., Furukawa, T., Yoshizato, K., 2004. Near completely humanized liver in mice shows human-type metabolic responses to drugs. Am. J. Pathol. 165, 901–912.
Tavangar, K., Hoffman, A.R., Kraemer, F.B., 1990. A micromethod for the isolation of total RNA from adipose tissue. Anal. Biochem. 186, 60–63.
Turesky, R.J., 2005. Interspecies metabolism of heterocyclic aromatic amines and the uncertainties in extrapolation of animal toxicity data for human risk assessment. Mol. Nutr. Food Res. 49, 101–117.
Uno, S., Dalton, T.P., Dragin, N., Curran, C.P., Derkenne, S., Miller, M.L., Shertzer, H.G., Gonzalez, F.J., Nebert, D.W., 2006. Oral benzo[*a*]pyrene in *Cyp1* knockout mouse lines: CYP1A1 important in detoxication, CYP1B1 metabolism required for immune damage independent of total-body burden and clearance rate. Mol. Pharmacol. 69, 1103–1114.
Uno, S., Dragin, N., Miller, M.L., Dalton, T.P., Gonzalez, F.J., Nebert, D.W., 2008. Basal and inducible CYP1 mRNA quantitation and protein localization throughout the mouse gastrointestinal tract. Free Radic. Biol. Med. 44, 570–583.
Wilson, M.D., Barbosa-Morais, N.L., Schmidt, D., Conboy, C.M., Vanes, L., Tybulewicz, V.L., Fisher, E.M., Tavaré, S., Odom, D.T., 2008. Species-specific transcription in mice carrying human chromosome 21. Science 322, 434–438.
Winer, J., Jung, C.K., Shackel, I., Williams, P.M., 1999. Development and validation of real-time quantitative reverse transcriptase-polymerase chain reaction for monitoring gene expression in cardiac myocytes in vitro. Anal. Biochem. 270, 41–49.

Inhibition of Transforming Growth Factor β Signaling by Halofuginone as a Modality for Pancreas Fibrosis Prevention

Orit Zion, MSc, Olga Genin, MSc,* Norifumi Kawada, MD,† Katsutoshi Yoshizato, MD,‡ Suzy Roffe, MsC,§ Arnon Nagler, MD,|| Juan L. Iovanna, MD, PhD,¶ Orna Halevy, PhD,§ and Mark Pines, PhD**

Objectives: Chronic pancreatitis is characterized by inflammation and fibrosis. We evaluated the efficacy of halofuginone, an inhibitor of collagen synthesis and myofibroblast activation, in preventing cerulein-induced pancreas fibrosis.

Methods: Collagen synthesis was evaluated by in situ hybridization and staining. Levels of prolyl 4-hydroxylase β (P4Hβ), cytoglobin/stellate cell activation–associated protein (Cygb/STAP), transgelin, tissue inhibitors of metalloproteinases, serum response factor, transforming growth factor β (TGFβ), Smad3, and pancreatitis-associated protein 1 (PAP-1) were determined by immunohistochemistry. Metalloproteinase activity was evaluated by zymography.

Results: Halofuginone prevented cerulein-dependent increase in collagen synthesis, collagen cross-linking enzyme P4Hβ, Cygb/STAP, and tissue inhibitors of metalloproteinase 2. Halofuginone did not affect TGFβ levels in cerulein-treated mice but inhibited serum response factor synthesis and Smad3 phosphorylation. In culture, halofuginone inhibited pancreatic stellate cell (PSC) proliferation and TGFβ-dependent increase in Cygb/STAP and transgelin synthesis and metalloproteinase 2 activity. Halofuginone increased c-Jun N-terminal kinase phosphorylation in PSCs derived from cerulein-treated mice. Halofuginone prevented the increase in acinar cell proliferation and further increased the cerulein-dependent PAP-1 synthesis.

Conclusions: Halofuginone inhibits Smad3 phosphorylation and increases c-Jun N-terminal kinase phosphorylation, leading to the inhibition of PSC activation and consequent prevention of fibrosis. Halofuginone increased the synthesis of PAP-1, which further reduces pancreas fibrosis. Thus, halofuginone might serve as a novel therapy for pancreas fibrosis.

Key Words: myofibroblasts, pancreatic stellate cells, Smad, collagen, transgelin, cytoglobin

(*Pancreas* 2009;38: 427–435)

Chronic pancreatitis is a progressive disease, characterized by inflammation, fibrosis, and atrophy of the gland tissue, which results in impaired exocrine and endocrine functions of the pancreas.[1] The cellular mechanisms governing pancreas fibrosis are shared among the various insults and, in many aspects, mirror the scarring and wound-healing processes of other tissues. Pancreas fibrosis, regardless of the cause, is characterized by an increase in extracellular matrix (ECM) constituents, although their relative distribution within the pancreas varies with the site and nature of the insult.[2] In the injured pancreas, the pancreatic stellate cells (PSCs) constitute the major source of ECM proteins.[3] These cells are usually quiescent, with a low proliferation rate; however, upon activation, they differentiate into myofibroblastlike cells with high proliferative capacity. The activated PSCs migrate to sites of tissue damage, where they synthesize ECM components to promote tissue repair.[4] The intracellular signaling mechanisms regulating PSC activation include the mitogen-activated protein kinase (MAPK) pathway, which plays a major role in ethanol- and acetaldehyde-dependent activation of PSC, phosphatidylinositol-3-kinase, and protein kinase C.[5]

The transition to the myofibroblastlike phenotype is associated with increased expression of specific smooth muscle genes such as α smooth muscle actin and transgelin (SM22α) and of specific markers such as cytoglobin/stellate cell activation–associated protein (Cygb/STAP) in fibrotic lesions of the pancreas.[6] Pancreatic stellate cells can be activated directly by alcohol consumption[7] or by cytokines derived from the immigrating inflammatory cells.[8,9] Platelet-derived growth factor is the major promoter of PSC migration, whereas transforming growth factor β (TGFβ) affects ECM production via a Smad-associated pathway. Upon phosphorylation by the TGFβ receptor, Smad3 enters the nucleus to modulate the transcription of target genes.[10] Smad3 links TGFβ signaling directly to the serum response factor (SRF)–associated regulatory network that controls the expression of smooth muscle–specific genes.[11,12] The predominant ECM protein synthesized by the PSCs is collagen type I, although increases in the gene expression of other types of collagens and other matrix proteins have also been reported.[13] Pancreas fibrosis may also result from a relative imbalance between the production and degradation of matrix proteins.[14] The PSCs constitute the source of various matrix metalloproteinases (MMPs) and tissue inhibitors of MMPs (TIMPs), which are necessary for ECM remodeling under the control of TGFβ.[15,16]

In addition to the morbidity and mortality caused by chronic pancreatitis, patients with this disease also have a substantially increased risk of developing pancreatic cancer. The PSCs play a major role in the growth and development of pancreas adenocarcinoma, which has a remarkable fibrotic component regulated by the TGFβ pathway.[4,17,18] The desmoplasia is created by activated PSCs, which are stimulated by the cancer cells, thereby influencing tumor aggressiveness.[19] Given that activated PSCs not only are the principal effector cells in pancreas fibrosis but also play a major role in pancreas carcinoma, it seems that targeting the fibroblast-to-PSC transition might be a promising therapeutic approach, for which there is a great unmet need.

From the *Institute of Animal Sciences, The Volcani Center, Bet Dagan, Israel; †Department of Hepatology, Graduate School of Medicine, Osaka City University, Japan; ‡Developmental Biology Laboratory, CLUSTER Project, and 21st Century COE Program, Department of Biological Science, Graduate School of Science, Hiroshima University, Japan; §Department of Animal Sciences, The Hebrew University of Jerusalem, Rehovot, Israel; ||Department of Hematology and Bone Marrow Transplantation, Chaim Sheba Medical Center, Tel Hashomer, Israel; and ¶INSERM U624, Stress Cellulaire, Campus de Luminy, Marseille, France.

Received for publication July 23, 2008; accepted November 24, 2008.

Reprints: Mark Pines, PhD, Institute of Animal Science, ARO, The Volcani Center, Bet Dagan 50250, Israel (e-mail: pines@agri.huji.ac.il).

Halofuginone, an analog of the plant alkaloid febrifugine, has been found to inhibit the activation of hepatic stellate cells (HSCs)[20,21] and the stromal fibroblast-to-myofibroblast transition in the tumor microenvironment.[22] Halofuginone overcame TGFβ-induced collagen synthesis by inhibiting Smad3 phosphorylation downstream of the TGFβ signaling pathway.[23] In animal models in which excess collagen is the hallmark of the disease, halofuginone prevented the increase in collagen synthesis. These models included mice afflicted with chronic graft-versus-host disease and tight-skin mice, rats with pulmonary fibrosis, and rats that developed adhesions at various sites.[23–25] When given to rats that exhibited established fibrosis, halofuginone caused almost a complete resolution of the fibrotic condition.[20] In addition, halofuginone markedly improved the capacity of a cirrhotic liver to regenerate after partial hepatectomy[26] by affecting the expression of early genes of liver regeneration under the control of TGFβ.[27,28] Topical treatment with halofuginone of a patient with chronic graft-versus-host disease and of patients with scleroderma elicited a transient attenuation of collagen α_1(I) gene expression and improvements in skin scores, thus demonstrating human clinical efficacy.[25,29]

In the present study, we evaluated the efficacy of halofuginone in inhibiting pancreas fibrosis in mice, with particular emphasis on TGFβ-dependent PSC activation and ECM production.

MATERIALS AND METHODS

Materials

Halofuginone bromhydrate was obtained from Collgard Biopharmaceuticals Ltd (Tel Aviv, Israel). Cerulein and β-casein were from Sigma (St Louis, Mo). Antibodies to Cygb/STAP were prepared according to Nakatani et al.[6] Smad3 and phosphorylated Smad3 (P-Smad3) antibodies were from Abcam (Cambridge, United Kingdom). Serum response factor antibodies were from Santa Cruz Biotechnology Inc (Santa Cruz, Calif). The proliferating cell nuclear antigen (PCNA) staining kit was from Zymed Laboratories (San Francisco, Calif). Metalloproteinase 2 and P4Hβ monoclonal antibodies were from Acris (Hiddenhausen, Germany), and TIMP1 and TIMP2 monoclonal antibodies were from Lab Vision (Fremont, Calif). Polyclonal antibodies to phospho-Akt (S^{473}P-AKT), phospho-ERK/MAPK (P-p44), total Akt and total ERK/MAPK (p44), and monoclonal antibody to total c-Jun N-terminal kinase (JNK) 1 were from Cell Signaling Technologies (Danvers, Mass). Active-JNK (P-JNK1) and active p38 (P-p38) antibodies were from Promega (Madison, Wis). Rabbit polyclonal antibodies against human pancreatitis-associated protein 1 (PAP-1) were prepared as described previously.[30]

Animal Model of Pancreas Fibrosis

Male ICR mice (Harlan Laboratories, Jerusalem, Israel) were kept under standard conditions with free access to water and chow. Fibrosis was induced in mice (n = 10) by repeated (every 6 h) intraperitoneal injections of cerulein (50 μg/kg) twice weekly for 4 or 8 weeks according to Neuschwander-Tetri et al.[31] Halofuginone was administered intraperitoneally to mice (n = 10) at 4 μg per animal, 3 times per week as described by Bruck et al,[20] starting at the same time as the cerulein. Untreated mice (n = 10) and mice treated only with halofuginone (n = 10) were used as controls. All animal experiments were carried out according to the guidelines of the Volcani Center Institutional Committee for Care and Use of Laboratory Animals (Bet Dagan, Israel).

Preparation of Sections, In Situ Hybridization, and Immunohistochemistry

Pancreas samples were fixed overnight in 4% paraformaldehyde in phosphate-buffered saline at 4°C. Serial 5-μm sections were prepared after the samples had been embedded in Paraplast (McCormick Scientific, St Louis, Mo). Collagenous and noncollagenous proteins were differentially stained with 0.1% Sirius red and 0.1% Fast green as a counterstain, in saturated picric acid. By this procedure, collagen is stained red. Collagen levels were quantified by image analysis (ImagePro; Media Cybernetics, Silver Spring, Md). At least 20 photographs were taken for each analysis per each treatment at each time point. The results were calculated as the red area divided by the total red and green area and presented as arbitrary units of the mean (SE). Special care was taken to exclude the blank areas, which probably represented artifacts. In situ hybridization with a digoxigenin-labeled collagen α_1(I) probe was performed as described by Bruck et al.[20] No signal was observed with the sense probe. For immunohistochemistry, the following antibodies were used: SRF (diluted 1:500), TGFβ1 (1:400), Cygb/STAP (1:700), Smad3 (1:200), P-Smad2/3 (1:700), P4Hβ (1:25), TIMP1 (1:50), TIMP2 (1:250), and PAP-1 (1:10). In all cases, at least 5 slides from all the animals within the group were evaluated blindly to the animal grouping.

Cell Culture

Pancreatic stellate cells were prepared from either control mice or mice treated with a single injection of cerulein (50 μg/kg). After 24 hours, the pancreas was excised, freed from fat and lymph nodes, and digested with collagenase IV (0.02%), and the resulting cell suspension was centrifuged at 1200*g* for 5 minutes. The cells were washed and resuspended in Dulbecco's modified essential medium (DMEM) containing 10% fetal bovine serum and antibiotics (100-U/mL penicillin, 100-mg/mL streptomycin) and plated on 6-well plates with the same medium.[32] No significant differences were observed in the cell yield between the control and cerulein-treated mice, and almost all the cells were stained positive for Cygb/STAP or SM22α. All of the cells were incubated at 37°C in a humidified atmosphere containing 5% carbon dioxide. The cells were incubated with serum-free DMEM for 6 hours and were then treated with fresh medium containing halofuginone (20 or 50 nmol/L), TGFβ (3 ng/mL), or both for an additional 24 hours. Cellular viability was determined by trypan blue exclusion. At the end of the incubation period, the cells were either counted directly with a cell counter (Coulter Electronics, Bath, United Kingdom) or resuspended in 500 μL of lysis buffer consisting of 1-mmol/L EDTA, 50-mmol/L Tris (pH, 7.5), 150-mmol/L NaCl, 10% glycerol, 1% Nonidet P40, and a 1:100 dilution of protease and phosphatase inhibitor cocktail (Sigma).

Western Blot

Protein lysate (30 μg) from either tissue or cells was electrophoresed on a 10% sodium dodecyl sulfate–polyacrylamide gel and transferred onto a nitrocellulose membrane. Nonspecific binding sites were blocked with 5% low-fat milk, and the membranes were incubated overnight with the appropriate antibodies for SM22α (1:5000), Cygb/STAP (1:1000), MMP-2 (1:200), phospho-Akt (1:1000), phosphor–ERK/MAPK (1:2000), total Akt and total ERK/MAPK (1:1500), active

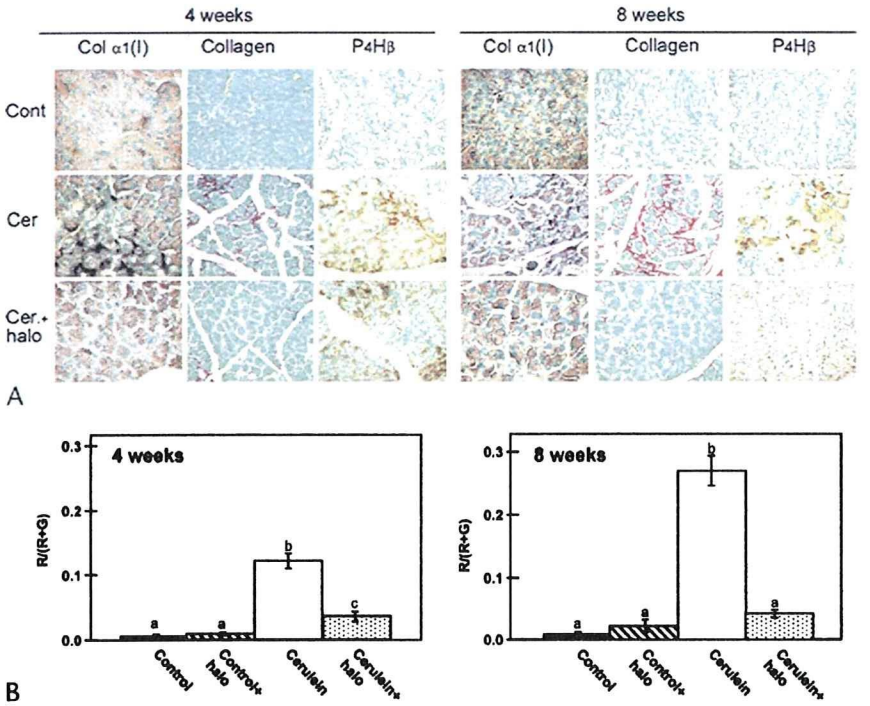

FIGURE 1. Effect of halofuginone on cerulein-dependent synthesis of collagen and P4Hβ, a collagen cross-linking enzyme. Mice were treated with cerulein for 4 or 8 weeks with or without halofuginone, after which pancreas biopsies were taken for histology. A, Collagen α_1(I) gene expression was determined by in situ hybridization, collagen level was evaluated by Sirius red staining, and P4Hβ was determined by immunohistochemistry. B, Image analysis of pancreas collagen levels. In each column, means without a common letter differ significantly ($P < 0.05$) according to Duncan multiple range test.

JNK (1:5000), active p38 (1:2000), and monoclonal antibody to total JNK (1:1000).

Zymography

Conditioned medium samples were analyzed for MMP activity, which was determined in a 10% sodium dodecyl sulfate–polyacrylamide gel impregnated with gelatin (0.01%) or β-casein (1.0 mg/mL). Proteins were separated on the gel under nonreducing conditions, followed by 1 hour of incubation in 2.5% Triton X-100 and 16 hours of incubation in 50-mmol/L Tris (pH, 7.6), 0.2-mol/L NaCl, and 5-mmol/L $CaCl_2$ at 37°C. After the incubation period, the gels were stained with 0.5% Coomassie G 250 in methanol/acetic acid/water (30:10:60, vol/vol/vol).

Statistical Analysis

The results are presented as the mean (SD). The significance of differences among different groups was determined by analysis of variance. In each column, means without a common letter differ significantly ($P < 0.05$) according to Duncan multiple range test.

RESULTS

Halofuginone Inhibits Pancreas Fibrosis

Pancreas fibrosis is the result of a dynamic cascade of mechanisms beginning with acinar cell injury and followed by inflammation and PSC activation. After 4 weeks of cerulein treatment, we observed a major increase in the number of PSCs expressing the collagen α_1(I) gene, the synthesis of large quantities of collagen surrounding the acinar cells, and positive staining for P4Hβ, one of the major enzymes responsible for collagen cross-linking and maturation (Fig. 1A). Collagen accumulated in the pancreas with time, and after an additional 4 weeks of cerulein treatment, a further increase in collagen content and P4Hβ level was observed. Halofuginone prevented the increase in fibrosis in a time-dependent fashion, as demonstrated by reductions in the expression of the collagen α_1(I) gene, in collagen content, and in the level of P4Hβ. After 4 weeks of halofuginone treatment, the collagen level was significantly lower than that of the cerulein-treated mice but was still higher than that of the control mice. After 8 weeks of halofuginone treatment, the collagen level was significantly lower than that of the cerulein-treated mice and did not differ from that of the control untreated mice (Fig. 1B). Halofuginone alone had no effect on the collagen content or other histologic parameters in the control untreated mice (data not shown).

Halofuginone Inhibits PSC Activation

In addition to enhancing collagen synthesis, activated PSCs are also characterized by increased proliferation and expression of SM22α and Cygb/STAP genes under the control of TGFβ. After 4 weeks of cerulein treatment, a major increase in the number of PSCs exhibiting Cygb/STAP was observed, which persisted for at least 8 weeks. Halofuginone reduced the number of Cygb/STAP-positive cells in the pancreas (Fig. 2A) and inhibited the TGFβ-induced Cygb/STAP levels in primary PSCs in cultures derived from the pancreas of control and cerulein-treated mice (Fig. 2B). Transgelin is induced during transdifferentiation of fibroblasts to myofibroblasts at the time of stromal tissue remodeling under the

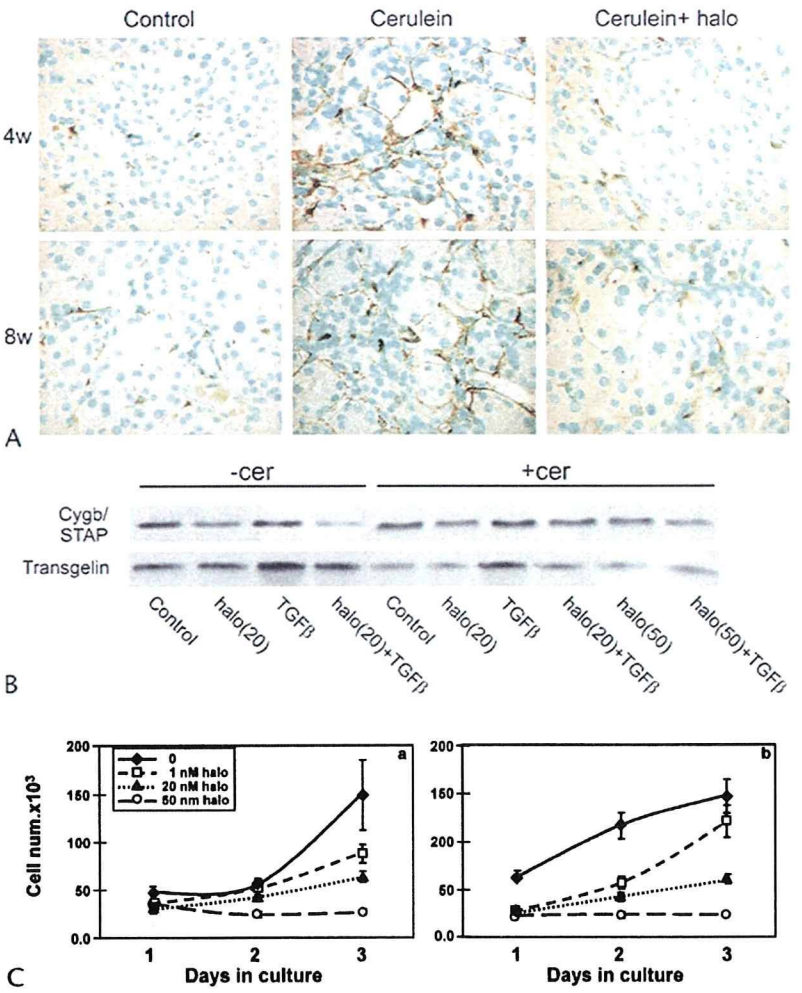

FIGURE 2. Effect of halofuginone on the synthesis of Cygb/STAP and SM22α and on PSC proliferation. A, Immunohistochemistry of Cygb/STAP in pancreas biopsies of mice treated for 4 or 8 weeks with cerulein, with or without halofuginone. B, Western blotting of Cygb/STAP and SM22α of PSCs derived from either control or cerulein-treated mice. The cells were incubated for 18 hours with TGFβ (3 ng/mL), halofuginone, or their combination. C, Primary PSCs were incubated with various concentrations of halofuginone, and cell proliferation was estimated directly by cell counting.

control of TGFβ. The PSCs in culture from control and cerulein-treated mice synthesized SM22α, which was upregulated by TGFβ. Halofuginone prevented the TGFβ-dependent SM22α synthesis in cultured primary PSCs derived from either control or cerulein-treated mice (Fig. 2B). The inhibitory effect of halofuginone on Cygb/STAP and SM22α synthesis was accompanied by a dose-dependent inhibition of proliferation of PSCs derived from either the normal pancreas or cerulein-treated mice (Fig. 2C). All of these findings were consistent with halofuginone inhibition of PSC activation.

Halofuginone and Matrix Degradation

The levels of TIMP1 and TIMP2 were increased in the pancreas after cerulein treatment, but only the TIMP2 level was inhibited by halofuginone (Fig. 3A). Metalloproteinase 2 is one of the major MMPs involved in pancreas fibrosis under the control of TGFβ.[14–16] Halofuginone had only a minimal, if any, effect on MMP-2 levels in the control mice. Cerulein treatment caused an increase in MMP-2 levels, which were further increased after halofuginone treatment (Fig. 3B). In culture, a major increase in basal MMP-2 activity was observed in conditioned medium of PSCs derived from cerulein-treated mice compared with controls (Fig. 3C). Halofuginone had no effect on the basal level of MMP-2 activity but inhibited the TGFβ-dependent increase in its activity by PSCs derived from control and cerulein-treated mice (Fig. 3D). In contrast, halofuginone increased MMP-3 activity, but only in PSCs derived from cerulein-treated mice (Fig. 3E).

Halofuginone Inhibits TGFβ Signaling

Almost no TGFβ was observed in the control untreated pancreas, whereas in the cerulein-treated mice, a major increase in its level was observed, mostly in the acinar cells but also in some of the PSCs (Fig. 4). Halofuginone treatment did not cause any change in the level of TGFβ, in agreement with previous studies suggesting that halofuginone affects TGFβ signaling downstream in its pathway.[23] Halofuginone treatment eliminated the synthesis of SRF, which was observed exclusively in the PSCs of the cerulein-treated pancreas. In the untreated pancreas, Smad3 was observed only in endothelial cells

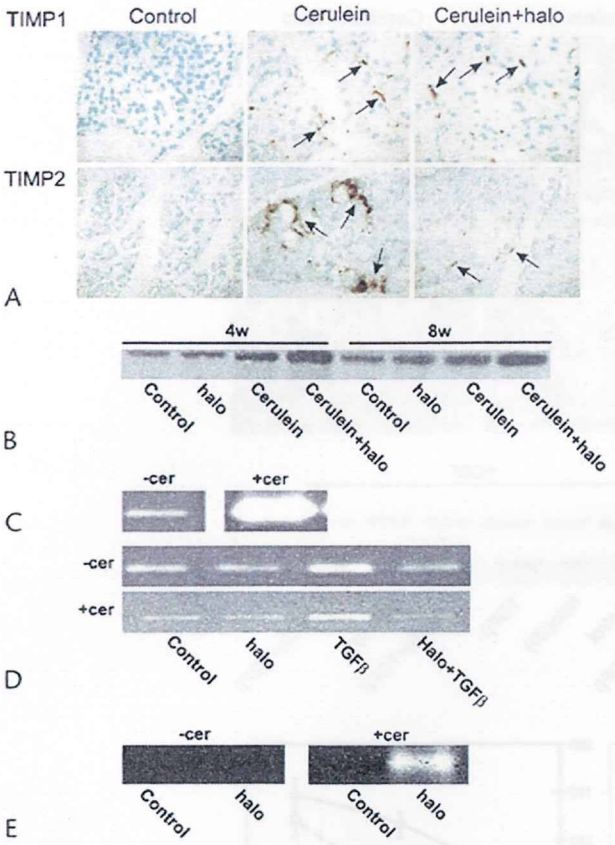

FIGURE 3. Halofuginone and the ECM degradation pathway. A, Immunohistochemistry of TIMP1 and TIMP2 in the pancreas after 8 weeks of cerulein treatment, with or without halofuginone. B, Western blotting with MMP-2 antibodies of pancreas extracts. C, Gelatin zymography for evaluation of MMP-2 activity in conditioned medium of PSCs derived from the cerulein-treated or untreated pancreas. Note the high levels of MMP-2 activity in conditioned medium of PSCs derived from the cerulein-treated pancreas. D, Effect of halofuginone on MMP-2 activity. E, Metalloproteinase 3 in conditioned medium collected from PSCs derived from the normal and the cerulein-treated pancreas.

surrounding the blood vessels, and no P-Smad3 was observed in any cell type. After cerulein treatment, increases in Smad3 and P-Smad3 were observed. Smad3 was observed mostly in the PSCs, whereas P-Smad3 was observed in the acinar cells and the PSCs. Halofuginone had no effect on the level of Smad3 protein expression, whereas complete elimination of P-Smad3 was observed after halofuginone treatment (Fig. 4).

Intracellular PSC Signaling Is Affected by Halofuginone

We evaluated the effect of halofuginone on the phosphorylation of key proteins in the MAPK pathways—JNK, MAPK/ERK, and p38 MAPK—and on Akt in PSCs derived from the control and the cerulein-treated pancreas (Fig. 5). Levels of phosphorylated JNK and, to a much lesser extent, phosphorylated MAPK/ERK were higher in the PSCs derived from the cerulein-treated pancreas relative to controls and were further increased after halofuginone treatment. Equal levels of phosphorylated Akt and p38 MAPK were observed in PSCs derived from control and cerulein-treated mice and were unaltered after halofuginone treatment.

Halofuginone Affects Cerulein-Dependent Acinar Cell Proliferation and PAP-1 Synthesis

Fully differentiated pancreatic acinar cells are capable of replication and can reenter the cell cycle to restore lost acinar tissue.[44] Only a small number of PCNA-positive acinar cells were detected in the untreated pancreas, whereas after cerulein treatment, a major increase in PCNA-positive cells was observed (Fig. 6). Halofuginone prevented this increase only in the early stages of pancreas fibrosis development. In pathologic situations, the acinar cells are the main source of PAP-1.[33] Almost no PAP-1 was synthesized by the control untreated pancreas or by the pancreas of mice treated with halofuginone alone. Cerulein caused increased PAP-1 synthesis, which was more evident after 4 weeks of treatment, and halofuginone caused a further increase in this synthesis (Fig. 7).

DISCUSSION

Chronic pancreatitis is characterized by pancreatic inflammation and fibrosis, eventually leading to destruction of pancreatic parenchyma and loss of exocrine and endocrine functions. In response to pancreatic injury or inflammation, PSCs are activated into highly proliferative myofibroblastlike cells that express smooth muscle proteins and produce ECM components. Administration of cerulein caused a major increase in the synthesis of fibrosis-related and TGFβ-dependent proteins such as collagen type I and P4Hβ (Fig. 1), consistent with other models of pancreatitis.[34,35] Halofuginone inhibited PSC activation, in agreement with previous observations of inhibition of HSC and tumor myofibroblast activation,[20,22,23] as evidenced by the following findings. (1) There was inhibition of synthesis of collagen type I, the major ECM protein, and of P4Hβ, the main enzyme responsible for its cross-linking (Fig. 1). The Sirius red staining that remained after halofuginone treatment may partly represent collagen type III, which also increases in pancreas fibrosis[35] but is not affected by halofuginone.[36] Halofuginone also inhibited collagen synthesis in severe hyperstimulation and obstruction pancreatitis in rats.[37] (2) There was inhibition of the expression of specific markers expressed in activated PSCs, such as Cygb/STAP, and of TGFβ-dependent increases in muscle-specific genes such as SM22α (Figs. 2A, B). (3) There was inhibition of PSC proliferation (Fig. 2C). All of the inhibited parameters are characteristic of activated PSCs. Transforming growth factor β is known to regulate PSC activation and to inhibit its proliferation. Although halofuginone inhibited TGFβ signaling, incubation of the PSC with halofuginone resulted in a dose-dependent inhibition of cell proliferation (Fig. 2C). These results suggest that halofuginone may have additional targets involved in cell proliferation, for example, within the MAPK signaling pathway (Fig. 5).

The course of chronic pancreatitis is characterized by recurrent episodes of acute pancreatitis, which cause parenchymal injury and necrosis, accompanied by fibrosis, chronic inflammation, and parenchymal cell loss, all of which increase with each successive episode. Hypoxia and hypoxia-related genes are upregulated during cerulein-induced acute pancreatitis.[38] It is interesting to note that the synthesis of Cygb/STAP and collagen P4Hβ is controlled by hypoxia.[39,40] Cytoglobin/stellate cell activation–associated protein is probably involved in cellular oxygen homeostasis and supply and plays a role as an oxygen reservoir that is used under hypoxic conditions to protect the tissue from oxidative stress.[41]

Regardless of the cause of the insult resulting in pancreas fibrosis, extensive ECM remodeling is required. In the first

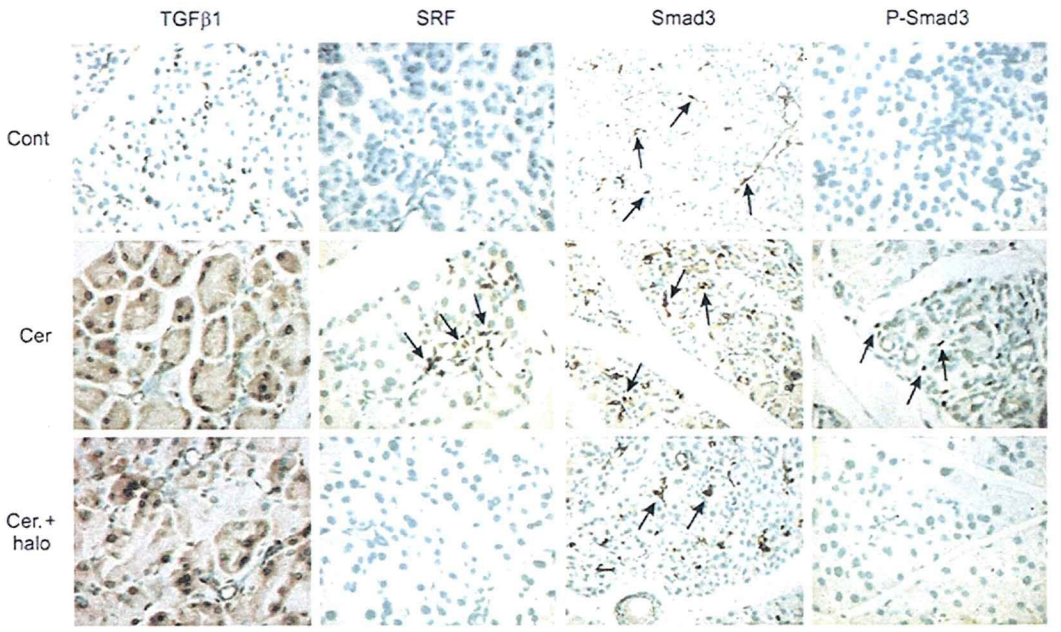

FIGURE 4. Halofuginone and TGFβ signaling. Transforming growth factor β, SRF, Smad3, and P-Smad3 levels were determined by immunohistochemistry in pancreas biopsies after 8 weeks of cerulein treatment, with or without halofuginone. Cells expressing the specific proteins are indicated by arrows. Note that halofuginone did not affect TGFβ levels but prevented the cerulein-dependent increases in SRF and P-Smad3, but not Smad3, levels.

step, transient local degradation of the ECM occurs, either by proteases of the plasminogen or by the MMP systems. The balance between the MMPs and their inhibitors is pivotal in the remodeling of the ECM. Tissue inhibitors of MMP-1 and TIMP2, derived from the activated PSCs,[16] are increased in the pancreas of cerulein-treated mice (Fig. 3A). Although both TIMPs are under the control of TGFβ, the regulation of TIMP1 is probably not Smad3-dependent. The Smad-containing complexes do not interact with the promoter-proximal activator protein 1 site of TIMP1 that is required for TGFβ activation; therefore, TGFβ was able to stimulate TIMP1 synthesis in a Smad-knockout cell line.[42] This could explain the observation that halofuginone, an inhibitor of Smad3 phosphorylation downstream of TGFβ signaling[21,23] (Fig. 4), inhibited only the synthesis of TIMP2 but not that of TIMP1 (Fig. 3A), as has been observed in chemically induced liver fibrosis.[20] Pancreatic stellate cells have the capacity to synthesize a number of MMPs under the control of TGFβ.[16] The PSCs derived from cerulein-treated mice exhibited much higher MMP-2 activity than those derived from the control mice, and the difference persisted even after several passages in culture (Fig. 3C). This may imply a fundamental genomic change while they are in the fibrotic tissue, or it may reflect the disparity in their origin. Halofuginone prevented the TGFβ-dependent increase in MMP-2 activity in both cell populations (Fig. 3D), but it increased MMP-3 activity only in the cells derived from cerulein-treated mice. These results are consistent with the effects of halofuginone on MMP activity observed in HSCs in culture and in rat hepatic-induced fibrosis.[43]

Transforming growth factor β is synthesized by the PSCs and was upregulated in the cerulein-treated pancreas (Fig. 4). Halofuginone, which has been found to overcome TGFβ-induced collagen synthesis without affecting TGFβ receptor expression,[23] did not affect TGFβ levels in the cerulein-treated mice, suggesting that halofuginone's target is probably downstream of the TGFβ-receptor interaction, along the Smad3 pathway. Indeed, halofuginone decreased the levels of P-Smad2/3 in the cerulein-treated pancreas without affecting the total level of Smad3, in agreement with previous findings.[21,23] Smad3, in conjunction with SRF, is a major mediator of TGFβ signaling, which results in transcription of smooth muscle–specific genes.[11] Serum response factor induces smooth muscle cell (SMC) gene expression, and the dominant-negative mutant of SRF blocks TGFβ-induced SMC genes.[44] In activated HSCs, TGFβ upregulates SRF synthesis, resulting in SMC gene expression.[45] The entire conditional inactivation of the SRF gene in the pancreas leads to severe pancreatitis,[46] although in the present study, in the cerulein-treated pancreas, SRF was upregulated exclusively by the PSCs, probably because of cerulein-dependent increases in TGFβ synthesis and Smad3 phosphorylation (Fig. 4). Halofuginone inhibited SRF synthesis without affecting the level of TGFβ, which again suggests that halofuginone inhibits smooth muscle gene expression and ECM production by inhibiting Smad3 phosphorylation downstream of TGFβ signaling, resulting in inhibition of PSC activation.

The PSCs derived from the pancreas of cerulein-treated mice exhibited much higher levels of phosphorylated JNK and, to a lesser extent, of MAPK/ERK, but not of p38 kinase or Akt. Halofuginone further increased JNK phosphorylation in the cerulein-treated PSCs. The JNK has been implicated as a repressor of TGFβ gene expression, and it contributes to the regulation of autocrine TGFβ-mediated biologic responses,[47] suggesting that there is cross-talk between the 2 signaling pathways. It is interesting to note that halofuginone causes increased phosphorylation of c-Jun transcription factor, a major JNK substrate, in Tsk/+ mouse fibroblasts in culture and in vivo, in correlation with a decrease in collagen synthesis.[48]

Halofuginone affects not only the stellate cells but also the epithelial cells of the tissue. In the liver, halofuginone stimulates insulin growth factor binding protein 1 synthesis by the hepatocytes, and the secreted insulin growth factor binding

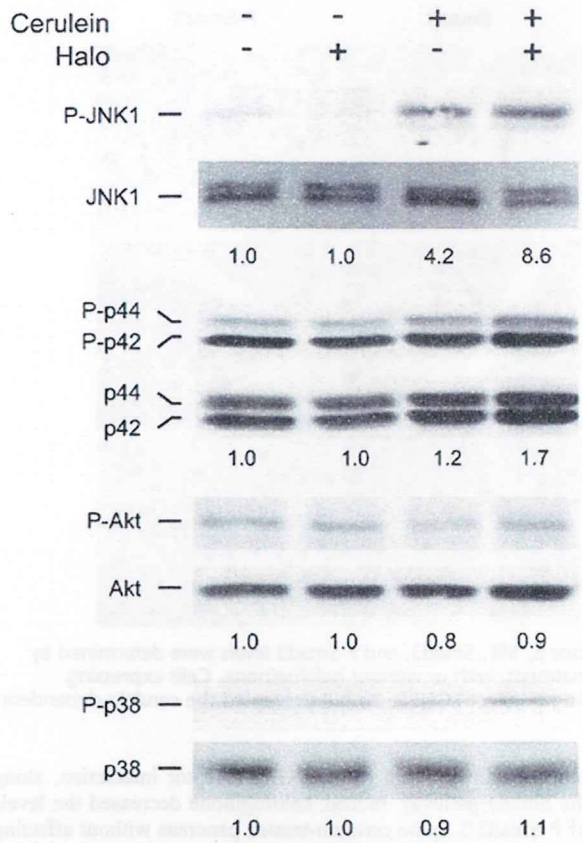

FIGURE 5. Halofuginone and JNK, MAPK, and Akt signaling in PSCs. Cells derived from the pancreas of control and cerulein-treated mice were cultured in the presence or absence of halofuginone (20 mmol/L). At the end of the incubation, cell extracts were blotted with the appropriate antibodies. Halofuginone further increased the cerulein-dependent phosphorylation of JNK and, to a lesser extent, the phosphorylation of MAPK/ERK. No effect of cerulein or halofuginone on Akt or p38 phosphorylation was observed.

protein 1 inhibits HSC migration.[27] In the pancreas, PAP-1 is expressed at a level related to the severity of cerulein-induced pancreatitis in the acute phase.[49] Halofuginone prevented the

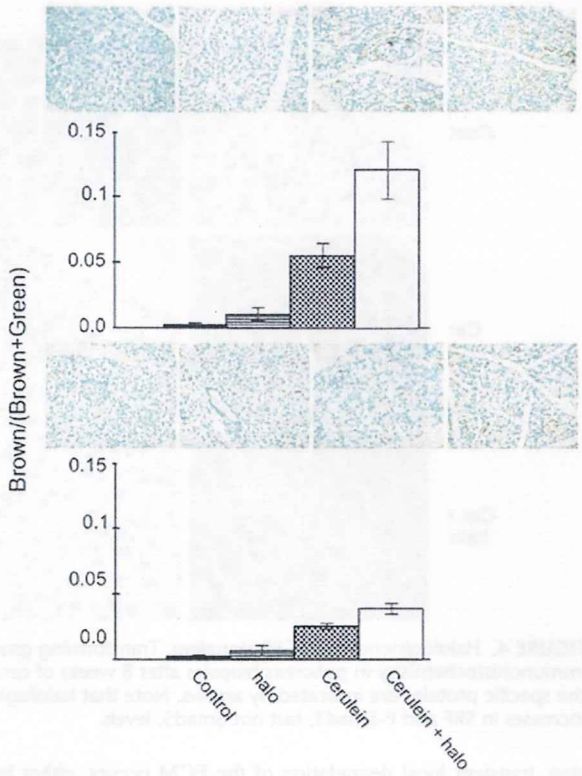

were taken after 4 and 8 weeks of cerulein treatment, with and without halofuginone, immunostained with PAP-1 antibodies, and subjected to image analysis. In each panel, means without a common letter differ significantly ($P < 0.05$) according to Duncan multiple range test.

cerulein-dependent increase in acinar cell proliferation and increased the synthesis of anti-inflammatory cytokine PAP-1 (Figs. 6, 7), which may further reduce PSC activation and matrix synthesis, by inhibiting inflammation. Halofuginone also inhibited rat inflammation after severe hyperstimulation and obstruction pancreatitis.[37]

In conclusion, we demonstrated that halofuginone prevents cerulein-dependent PSC activation by inhibiting Smad3

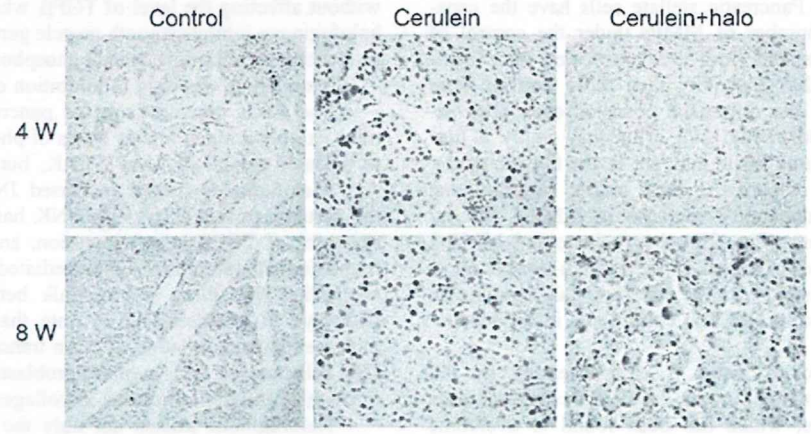

FIGURE 6. Halofuginone and acinar cell proliferation. Pancreas biopsies were taken after 4 and 8 weeks of cerulein treatment, with and without halofuginone, and were immunostained with PCNA antibodies. Halofuginone prevented the increase in acinar cell proliferation after only 4 weeks of treatment.

phosphorylation downstream of TGFβ signaling and via JNK phosphorylation. In addition, halofuginone increases the synthesis of the anti-inflammatory cytokine PAP-1 by the acinar cells, which can further reduce pancreas fibrosis. These results suggest that halofuginone, which has already exhibited human clinical efficacy[25,29] and is currently being evaluated in clinical trials for various indications,[50] could serve as a novel therapy for pancreas fibrosis.

ACKNOWLEDGMENT

This article is a contribution from the ARO, The Volcani Center.

REFERENCES

1. Witt H, Apte MV, Keim V, et al. Chronic pancreatitis: challenges and advances in pathogenesis, genetics, diagnosis, and therapy. *Gastroenterology.* 2007;132:1557–1573.
2. Kloppel G, Detlefsen S, Feyerabend B. Fibrosis of the pancreas: the initial tissue damage and the resulting pattern. *Virchows Arch.* 2004;445:1–8.
3. Apte MV, Wilson JS. Mechanisms of pancreatic fibrosis. *Dig Dis.* 2004;22:273–279.
4. Bachem MG, Schunemann M, Ramadani M, et al. Pancreatic carcinoma cells induce fibrosis by stimulating proliferation and matrix synthesis of stellate cells. *Gastroenterology.* 2005;128:907–921.
5. McCarroll JA, Phillips PA, Park S, et al. Pancreatic stellate cell activation by ethanol and acetaldehyde: is it mediated by the mitogen-activated protein kinase signaling pathway? *Pancreas.* 2003;27:150–160.
6. Nakatani K, Okuyama H, Shimahara Y, et al. Cytoglobin/STAP, its unique localization in splanchnic fibroblast-like cells and function in organ fibrogenesis. *Lab Invest.* 2004;84:91–101.
7. Apte MV, Phillips PA, Fahmy RG, et al. Does alcohol directly stimulate pancreatic fibrogenesis? Studies with rat pancreatic stellate cells. *Gastroenterology.* 2000;118:780–794.
8. Luttenberger T, Schmid-Kotsas A, Menke A, et al. Platelet-derived growth factors stimulate proliferation and extracellular matrix synthesis of pancreatic stellate cells: implications in pathogenesis of pancreas fibrosis. *Lab Invest.* 2000;80:47–55.
9. Yoo BM, Yeo M, Oh TY, et al. Amelioration of pancreatic fibrosis in mice with defective TGF-beta signaling. *Pancreas.* 1995;30:71–79.
10. Roberts AB, Russo A, Felici A, et al. Smad3: a key player in pathogenetic mechanisms dependent on TGF-beta. *Ann N Y Acad Sci.* 2003;995:1–10.
11. Qiu P, Feng XH, Li L. Interaction of Smad3 and SRF-associated complex mediates TGF-beta1 signals to regulate SM22 transcription during myofibroblast differentiation. *J Mol Cell Cardiol.* 2003;35:1407–1420.
12. Mack CP, Thompson MM, Lawrenz-Smith S, et al. Smooth muscle alpha-actin CArG elements coordinate formation of a smooth muscle cell–selective, serum response factor–containing activation complex. *Circ Res.* 2000;86:221–232.
13. Jesnowski R, Furst D, Ringel J, et al. Immortalization of pancreatic stellate cells as an in vitro model of pancreatic fibrosis: deactivation is induced by matrigel and *N*-acetylcysteine. *Lab Invest.* 2005;85: 1276–1291.
14. Ishihara T, Hayasaka A, Yamaguchi T, et al. Immunohistochemical study of transforming growth factor-beta 1, matrix metalloproteinase-2,9, tissue inhibitors of metalloproteinase-1,2, and basement membrane components at pancreatic ducts in chronic pancreatitis. *Pancreas.* 1998;17:412–418.
15. Yokota T, Denham W, Murayama K, et al. Pancreatic stellate cell activation and MMP production in experimental pancreatic fibrosis. *J Surg Res.* 2002;104:106–111.
16. Phillips PA, McCarroll JA, Park S, et al. Rat pancreatic stellate cells secrete matrix metalloproteinases: implications for extracellular matrix turnover. *Gut.* 2003;52:275–282.
17. Omary MB, Lugea A, Lowe AW, et al. The pancreatic stellate cell: a star on the rise in pancreatic diseases. *J Clin Invest.* 2007;117:50–59.
18. Hwang RF, Moore T, Arumugam T, et al. Cancer-associated stromal fibroblasts promote pancreatic tumor progression. *Cancer Res.* 2008;68:918–926.
19. Erkan M, Kleeff J, Gorbachevski A, et al. Periostin creates a tumor-supportive microenvironment in the pancreas by sustaining fibrogenic stellate cell activity. *Gastroenterology.* 2007;132:1447–1464.
20. Bruck R, Genina O, Aeed H, et al. Halofuginone to prevent and treat thioacetamide-induced liver fibrosis in rats. *Hepatology.* 2001;3: 379–386.
21. Gnainsky Y, Kushnirsky Z, Bilu G, et al. Gene expression during chemically induced liver fibrosis: effect of halofuginone on TGF-beta signaling. *Cell Tissue Res.* 2007;328:153–166.
22. Sheffer Y, Leon O, Pinthus JH, et al. Inhibition of fibroblast to myofibroblast transition by halofuginone contributes to the chemotherapy-mediated antitumoral effect. *Mol Cancer Ther.* 2007;6: 570–577.
23. Pines M. Targeting TGFβ signaling to inhibit fibroblast activation as a therapy for fibrosis and cancer: effect of halofuginone. *Exp Opion Drug Discov.* 2008;3:1–10.
24. Pines M, Vlodavsky I, Nagler A. Halofuginone: from veterinary use to human therapy. *Drug Develop Res.* 2000;50:371–378.
25. Pines M, Snyder D, Yarkoni S, et al. Halofuginone to treat fibrosis in chronic graft versus host disease and scleroderma. *Biol Bl Marrow Transplant.* 2003;9:417–425.
26. Spira G, Mawasi N, Paizi M, et al. Halofuginone, a collagen type I inhibitor improves liver regeneration in cirrhotic rats. *J Hepatol.* 2002;37:331–339.
27. Gnainsky Y, Spira G, Paizi M, et al. Halofuginone—an inhibitor of collagen synthesis by rat stellate cells—stimulates insulin-like growth factor-binding protein 1 synthesis by hepatocytes. *J Hepatol.* 2003;40: 269–277.
28. Gnainsky Y, Spira G, Paizi M, et al. The involvement of the tyrosine phosphatase early gene of liver regeneration (PRL-1) in cell cycle and in liver regeneration and fibrosis—effect of halofuginone. *Cell Tissue Res.* 2006;324:385–394.
29. Nagler A, Pines M. Topical treatment of cutaneous chronic graft versus host disease (cGvHD) with halofuginone: a novel inhibitor of collagen type I synthesis. *Transplantation.* 1999;68:1806–1809.
30. Keim V, Iovanna JL, Orelle B, et al. A novel exocrine protein associated with pancreas transplantation in humans. *Gastroenterology.* 1992;103:248–254.
31. Neuschwander-Tetri BA, Burton FR, Presti ME, et al. Repetitive self-limited acute pancreatitis induces pancreatic fibrogenesis in the mouse. *Dig Dis Sci.* 2000;45:665–674.
32. Kruse ML, Hildebrand PB, Timke C, et al. Isolation, long-term culture, and characterization of rat pancreatic fibroblastoid/stellate cells. *Pancreas.* 2001;23:49–54.
33. Closa D, Motoo Y, Iovanna JL. Pancreatitis-associated protein: from a lectin to an anti-inflammatory cytokine. *World J Gastroenterol.* 2007;13:170–174.
34. Koslowski R, Seidel D, Kuhlisch E, et al. Evidence for the involvement of TGF-beta and PDGF in the regulation of prolyl 4-hydroxylase and lysyloxidase in cultured rat lung fibroblasts. *Exp Toxicol Pathol.* 2003;55:257–264.

35. Miyauchi M, Suda K, Kuwayama C, et al. Role of fibrosis-related genes and pancreatic duct obstruction in rat pancreatitis models: implications for chronic pancreatitis. *Histol Histopathol.* 2007;22:1119–1127.

36. Choi ET, Callow AD, Sehgal NL, et al. Halofuginone, a specific collagen type I inhibitor, reduces anastomotic intimal hyperplasia. *Arch Surg.* 1995;130:257–261.

37. Karatas A, Paksoy M, Erzin Y, et al. The effect of halofuginone, a specific inhibitor of collagen type 1 synthesis, in the prevention of pancreatic fibrosis in an experimental model of severe hyperstimulation and obstruction pancreatitis. *J Surg Res.* 2008;148:7–12.

38. Gomez G, Englander EW, Wang G, et al. Increased expression of hypoxia-inducible factor-1alpha, p48, and the Notch signaling cascade during acute pancreatitis in mice. *Pancreas.* 2004;28:58–64.

39. Fähling M, Perlewitz A, Doller A, et al. Regulation of collagen prolyl 4-hydroxylase and matrix metalloproteinases in fibrosarcoma cells by hypoxia. *Comp Biochem Physiol C Toxicol Pharmacol.* 2004;139:119–126.

40. Fordel E, Thijs L, Martinet W, et al. Anoxia or oxygen and glucose deprivation in SH-SY5Y cells: a step closer to the unraveling of neuroglobin and cytoglobin functions. *Gene.* 2007;398:114–122.

41. Xu R, Harrison PM, Chen M, et al. Cytoglobin overexpression protects against damage-induced fibrosis. *Mol Ther.* 2006;13:1093–1100.

42. Hall MC, Young DA, Waters JG, et al. The comparative role of activator protein 1 and Smad factors in the regulation of Timp-1 and MMP-1 gene expression by transforming growth factor-beta 1. *J Biol Chem.* 2003;278:10304–10313.

43. Popov Y, Patsenker E, Bauer M, et al. Halofuginone induces matrix metalloproteinases in rat hepatic stellate cells via activation of p38 and NFkappaB. *J Biol Chem.* 2006;281:15090–15098.

44. Hirschi KK, Lai L, Belaguli NS, et al. Transforming growth factor-beta induction of smooth muscle cell phenotype requires transcriptional and post-transcriptional control of serum response factor. *J Biol Chem.* 2002;277:6287–6295.

45. Herrmann J, Haas U, Gressner AM, et al. TGF-beta up-regulates serum response factor in activated hepatic stellate cells. *Biochim Biophys Acta.* 2007;1772:1250–1257.

46. Miralles F, Hebrard S, Lamotte L, et al. Conditional inactivation of the murine serum response factor in the pancreas leads to severe pancreatitis. *Lab Invest.* 2006;86:1020–1036.

47. Ventura JJ, Kennedy NJ, Flavell RA, et al. JNK regulates autocrine expression of TGF-beta1. *Mol Cell.* 2004;15:269–278.

48. McGaha TL, Kodera T, Spiera H, et al. Halofuginone inhibition of COL1A2 promoter activity via a c-Jun–dependent mechanism. *Arthritis Rheum.* 2002;46:2748–2761.

49. Magaña-Gómez J, López-Cervantes G, Calderón de la Barca AM. Caerulin-induced pancreatitis in rats: histological and genetic expression changes from acute phase to recuperation. *World J Gastroenterol.* 2006;12:3999–4003.

50. de Jonge MJ, Dumez H, Verweij J, et al. EORTC New Drug Development Group (NDDG). Phase I and pharmacokinetic study of halofuginone, an oral quinazolinone derivative in patients with advanced solid tumours. *Eur J Cancer.* 2006;42:1768–1774.

Genomics xxx (2010) xxx–xxx

Contents lists available at ScienceDirect

Genomics

journal homepage: www.elsevier.com/locate/ygeno

Comprehensive gene expression analysis of 5′-end of mRNA identified novel intronic transcripts associated with hepatocellular carcinoma

Yuji Hodo [a], Shin-ichi Hashimoto [b], Masao Honda [a], Taro Yamashita [a], Yutaka Suzuki [c], Sumio Sugano [c], Shuichi Kaneko [a,*], Kouji Matsushima [b]

[a] Department of Gastroentelorogy, Kanazawa University Graduate School of Medical Science, 13-1 Takara-Machi, Kanazawa, Ishikawa 920-8641, Japan
[b] Department of Molecular Preventive Medicine, School of Medicine, The University of Tokyo, 7-3-1, Hongo, Bunkyo-ku, Tokyo 113-0033, Japan
[c] Department of Medical Genome Sciences, Graduate School of Frontier Sciences, The University of Tokyo, 5-1-5, Kashiwanoha, Kashiwa, Chiba 277-8562, Japan

ARTICLE INFO

Article history:
Received 1 June 2009
Accepted 14 January 2010
Available online xxxx

Keywords:
5′-end serial analysis of gene expression
Transcriptional start site
Acyl-coenzyme A oxidase 2
Intron
Hepatocellular carcinoma

ABSTRACT

To elucidate the molecular feature of human hepatocellular carcinoma (HCC), we performed 5′-end serial analysis of gene expression (5′SAGE), which allows genome-wide identification of transcription start sites in addition to quantification of mRNA transcripts. Three 5′SAGE libraries were generated from normal human liver (NL), non-B, non-C HCC tumor (T), and background non-tumor tissues (NT). We obtained 226,834 tags from these libraries and mapped them to the genomic sequences of a total of 8,410 genes using RefSeq database. We identified several novel transcripts specifically expressed in HCC including those mapped to the intronic regions. Among them, we confirmed the transcripts initiated from the introns of a gene encoding acyl-coenzyme A oxidase 2 (*ACOX2*). The expression of these transcript variants were up-regulated in HCC and showed a different pattern compared with that of ordinary *ACOX2* mRNA. The present results indicate that the transcription initiation of a subset of genes may be distinctively altered in HCC, which may suggest the utility of intronic RNAs as surrogate tumor markers.

Introduction

Hepatocellular carcinoma (HCC) is the fifth most common cancer worldwide and the third most common cause of cancer mortality. HCC usually develops in patients with virus-induced (e.g., hepatitis B virus (HBV) and hepatitis C virus (HCV)) chronic inflammatory liver disease [1]; however, non-B, non-C HCC has been reported in patients negative for both HBV and HCV [2]. HCC development is a multistep process involving changes in host gene expression, some of which are correlated with the appearance and progression of a tumor. Multiple studies linking hepatitis viruses and chemical carcinogens with hepatocarcinogesis have provided insights into tumorigenesis [1,3]. Nevertheless, the genetic events that lead to HCC development remain unknown, and the molecular pathogenesis of HCC in most patients is still unclear. Therefore, elucidation of the genetic changes specific to the pathogenesis of non-B, non-C HCC may be useful to reveal the molecular features of HCCs irrelevant to viral infection.

Gene expression profiling, either by cDNA microarray [4] or serial analysis of gene expression (SAGE) [5], is a powerful molecular technique that allows analysis of the expression of thousands of genes. In particular, SAGE enables the rapid, quantitative, and simultaneous monitoring of the expression of tens of thousands of genes in various tissues [6,7]. Although numerous studies using cDNA microarrays and SAGE have been performed to clarify the genomic and molecular alterations associated with HCC [6,8–10], most expression data have been derived from the 3′-end region of mRNA. Recent advances in molecular biology have enabled genome-wide analysis of the 5′-end region of mRNA that revealed the variation in transcriptional start sites [11,12] and the presence of a large number of non-coding RNAs [13]. These approaches might be useful for identifying the unique and undefined genes associated with HCC not identified by the analysis of the 3′-end region of mRNA. SAGE based on the 5′-end (5′SAGE), a recently developed technique, allows for a comprehensive analysis of the transcriptional start site and quantitative gene expression [14]. This article is to elucidate the molecular carcinogenesis of non-B, non-C HCCs, while those heterogeneous entities are supposed not to share the same etiology, by using 5′SAGE.

Results

Annotation of the 5′SAGE tags to the human genome

We characterized a total of 226,834 tags from three unique 5′SAGE libraries (75,268 tags from the normal liver (NL) library, 75,573 tags from the non-tumor tissue (NT) library, and 75,993 tags from the tumor (T) library) and compared them against the human genome

Abbreviations: 5′SAGE, 5′-end serial analysis of gene expression; HCC, hepatocellular carcinoma; ACOX2, acyl-coenzyme A oxidase 2.

* Corresponding author. Fax: +81 76 234 4250
E-mail address: skaneko@m-kanazawa.jp (S. Kaneko).

0888-7543/$ – see front matter © 2010 Published by Elsevier Inc.
doi:10.1016/j.ygeno.2010.01.004

sequence. A total of 211,818 tags matched genomic sequences, representing 104,820 different tags in the three libraries (Table 1). About 60–65% of these tags mapped to a single locus in the genome in each library. Then, we mapped these single-matched tags to the well-annotated genes using RefSeq database (www.ncbi.nlm.nih.gov/RefSeq/, reference sequence database developed by NCBI). A total of 45,601 tags from the NL library, 39,858 from the NT library, and 41,265 from the T library were successfully mapped to 8410 unique genes (4397 genes detected in the NL library, 5194 genes in the NT library, and 6304 genes in the T library).

Gene expression profiling of non-B, non-C HCC

Abundantly expressed transcripts in the NL library and their corresponding expression in the NT and T libraries are shown in Table 2. The most abundant transcript in all three libraries was encoded by the *albumin (ALB)* gene. Transcripts encoding apolipoproteins were also abundantly expressed in each library, suggesting the preservation of hepatocytic gene expression patterns in HCC. Of note, the expression of *haptoglobin (HP)* (NL: 631, NT: 329, T: 57) and *metallothionein 1G (MTIG)* (NL: 392, NT: 169, T: 2) was decreased in the NT library and more in T library compared with NL library. Furthermore, the expression of *metallothionein 2A (MT2A)* (NL: 1027, NT: 872, T: 19), *metallothionein 1X (MT1X)* (NL: 547, NT: 644, T: 11), and *metallothionein 1E (MT1E)* (NL: 275, NT: 340, T: 2) was decreased almost fifty-fold or more in the T library compared with the NL and NT libraries. In contrast, the expression of *ribosomal protein S29 (RPS29)* (NL: 372, NT: 1011, T: 1768) was increased in the NT library and more in T library compared with NL library. Thus, transcripts associated with a certain liver function including xenobiotic metabolism might be suppressed whereas those associated with protein synthesis might be expressed in non-B, non-C HCC, similar to that observed in HCV-HCC [15].

We then investigated the characteristics of gene expression patterns in non-B, non C HCC. Two hundred fifty-four and 172 genes were up- or down-regulated in the T library more than five-fold compared with the NL library (data not shown). The top 10 genes are listed in Table 3a, and we identified several novel genes not yet reported to be differentially expressed in non-B, non-C HCC. Representative novel gene expression changes identified by 5′SAGE were validated by semi-quantitative reverse transcriptase-polymerase chain reaction (RT-PCR) analysis (Supplemental Fig. 1). RT-PCR results showed that the expression of *galectin 4 (LGALS4)*, *X antigen family, member 1A (XAGE 1A)*, *retinol dehydrogenase 11 (RDH11)*, *hydroxysteroid (17-beta) dehydrogenase 14 (HSD17B14)* *transmembrane 14A (TMEM14A)*, *stimulated by retinoic acid 13 homolog (STRA13)*, and *dual specificity phosphatase 23 (DUSP23)* was increased, whereas the expression of *C-type lectin superfamily 4 member G (CLEC4G)* was decreased in HCC tissues compared with the non-tumor tissues.

To further characterize the gene expression patterns of non-B, non-C HCC comprehensively, we compared the Gene Ontology process of three types of HCCs (i.e., non-B, non-C HCC; HBV-HCC; HCV-HCC) based on our previously described data [16]. The pathway analysis using MetaCore™ software showed that the immune related and cell adhesion related pathways were up-regulated in HCV-HCC with statistically significance, and the insulin signaling and angiogenesis related pathways were up-regulated in HBV-HCC with statistically significance, confirming our previous results [16]. Interestingly, genes associated with progesterone signaling were up-regulated in non-B, non-C HCC, while genes associated with proteolysis in the cell cycle, apoptosis and the ESR1-nuclear pathway were up-regulated in all types of HCC (Supplemental Fig. 2).

Dynamic alteration of transcription initiation in HCC

Although various transcriptome analyses have discovered considerable gene expression changes in cancer, it is still unclear if transcription is differentially initiated and/or terminated in HCC compared with the non-cancerous liver. We therefore explored the characteristics of transcription initiation and/or termination in HCC using 5′SAGE and 3′ SAGE data. Markedly, we observed relevant differences between 5′SAGE and 3′SAGE data derived from the same HCC sample (Tables 3a and b). For example, a gene encoding *coagulation factor XIII, B polypeptide (F13B)* was 13-fold up-regulated at transcription start sites (5′SAGE) but two-fold down-regulated at transcription termination sites (3′SAGE). On the other hand, a gene encoding *adenylate cyclase 1 (ADCY1)* was 50-fold down-regulated at transcriptional termination sites (3′SAGE) but showed no difference at transcriptional start sites (5′SAGE). These data suggest the dramatic alteration of all process of transcription in HCC, and the transcripts initiated at certain sites might be specifically associated with and involved in HCC pathogenesis, which could be a novel marker for HCC diagnosis.

Identification of novel intronic transcripts in HCC

Recent lines of evidence suggest that the majority of sequences of eukaryotic genomes may be transcribed, not only from known transcription start sites but also from intergenic regions and introns [17,18]. Introns are recognized as a significant source of functional non-coding RNAs (ncRNAs) including microRNAs (miRNAs) [18]. Moreover, a recent report implied the role of some large intronic RNAs in the pathogenesis of several types of malignancies [19]. Thus, analysis of transcripts originating from introns might be valuable for elucidating the genetic traits of HCC. We therefore focused on the transcriptional start sites potentially initiated from the intron and deregulated in HCC using 5′SAGE data. We identified that 97% of 5′ SAGE tags annotated by the RefSeq database matched the sequences in the exons, while 3% matched those in the introns (1257 in the N library, 1225 in the NT library, and 1261 in the T library) (Table 4a). To identify the possible promoter regions located in the intron, we clustered the different SAGE tags to a certain genomic region if these tags positioned within 500 bp intervals (Supplemental Fig. 3), as described previously [12].

Table 1
Experimental matching of 5′SAGE tags to genome.

	Normal liver	Non-tumor	Tumor	Total
All tags	75,268	75,573	75,993	226,834
Tags mapped to genome (%)				
1 locus/genome	51,076 (71.2)	47,200 (68.0)	48,503 (68.5)	146,779 (69.3)
Multiple loci/genome	20,608 (28.8)	22,142 (32.0)	22,289 (31.5)	65,039 (30.7)
Total tags	71,684 (100)	69,342 (100)	70,792 (100)	211,818 (100)
Unique tags mapped to genome (%)				
1 locus/genome	20,736 (65.5)	20,487 (60.2)	23,753 (60.7)	64,976 (62.0)
Multiple loci/genome	10,914 (34.5)	13,548 (39.8)	15,382 (39.3)	39,844 (38.0)
Total tags	31,650 (100)	34,035 (100)	39,135 (100)	104,820 (100)
Total tags to RefSeq	45,601	39,858	41,265	126,724
Unique gene	4397	5194	6304	8410

5′SAGE indicates 5′-end serial analysis of gene expression.

Please cite this article as: Y. Hodo, et al., Comprehensive gene expression analysis of 5′-end of mRNA identified novel intronic transcripts associated with hepatocellular carcinoma, Genomics (2010), doi:10.1016/j.ygeno.2010.01.004

Table 2
The highly expressed genes in the NL library and corresponding expression in the NT and T libraries (top 50 from NL library).

Tag count			Ratio		Gene
NL	NT	T	NT/NL	T/NL	
3731	1716	2328	0.460	0.624	Albumin (ALB)
2484	2146	2042	0.864	0.822	Apolipoprotein C-I (APOC1)
1955	1603	1079	0.820	0.552	Apolipoprotein A-II (APOA2)
1653	1050	828	0.635	0.501	Apolipoprotein A-I (APOA1)
1252	1908	1203	1.524	0.961	Transthyretin (prealbumin, amyloidosis type I) (TTR)
1233	724	220	0.587	0.178	Serpin peptidase inhibitor, clade A, member 1 (SERPINA1)
1027	872	19	0.849	0.019	Metallothionein 2A (MT2A)
755	1144	762	1.515	1.009	Ferritin, light polypeptide (FTL)
713	632	680	0.886	0.954	Alpha-1-microglobulin/bikunin precursor (AMBP)
635	524	1336	0.825	2.104	Apolipoprotein E (APOE)
631	329	57	0.521	0.090	Haptoglobin (HP)
600	228	212	0.380	0.353	Fibrinogen gamma chain (FGG)
549	395	302	0.719	0.550	Apolipoprotein C-III (APOC3)
547	644	11	1.177	0.020	Metallothionein 1X (MT1X)
479	257	290	0.537	0.605	Tumor protein, translationally-controlled 1 (TPT1)
463	217	53	0.469	0.114	Serpin peptidase inhibitor, clade A, member 3 (SERPINA3)
393	204	206	0.519	0.524	Ribosomal protein L26 (RPL26)
392	169	2	0.431	0.005	Metallothionein 1G (MT1G)
372	1011	1768	2.718	4.753	Ribosomal protein S29 (RPS29)
306	163	223	0.533	0.729	Ribosomal protein S27 (RPS27)
279	135	159	0.484	0.570	Ribosomal protein S16 (RPS16)
275	340	2	1.236	0.007	Metallothionein 1E (MT1E)
269	170	246	0.632	0.914	Ribosomal protein S23 (RPS23)
260	142	92	0.546	0.354	Fibrinogen beta chain (FGB)
260	200	195	0.769	0.750	Aldolase B, fructose-bisphosphate (ALDOB)
255	228	286	0.894	1.122	Ribosomal protein S12 (RPS12)
248	162	198	0.653	0.798	Ribosomal protein S14 (RPS14)
246	175	70	0.711	0.285	Interferon induced transmembrane protein 3 (IFITM3)
239	198	273	0.828	1.142	Ribosomal protein L31(RPL31)
229	264	0	1.153	0.004	Hepcidin antimicrobial peptide (HAMP)
228	149	156	0.654	0.684	Ribosomal protein S20 (RPS20)
222	191	117	0.860	0.527	Ubiquitin B (UBB)
216	218	352	1.009	1.630	Ribosomal protein L41 (RPL41)
210	150	155	0.714	0.738	Ribosomal protein, large, P1(RPLP1)
201	110	90	0.547	0.448	Ribosomal protein, large, P2 (RPLP2)
198	102	64	0.515	0.323	Fibrinogen alpha chain (FGA)
196	143	408	0.730	2.082	Ribosomal protein L37 (RPL37)
192	123	56	0.641	0.292	Ribosomal protein L37a (RPL37A)
191	208	346	1.089	1.812	Ribosomal protein L30 (RPL30)
174	109	76	0.626	0.437	Ribosomal protein L35 (RPL35)
169	208	3	1.231	0.018	Cytochrome P450, family 2, subfamily E, polypeptide 1 (CYP2E1)
167	105	300	0.629	1.796	Apolipoprotein H (beta-2-glycoprotein I) (APOH)
162	106	33	0.654	0.204	Serum amyloid A4, constitutive (SAA4)
159	85	157	0.535	0.987	Ribosomal protein L34 (RPL34)
159	113	229	0.711	1.440	Transferrin (TF)
155	84	135	0.542	0.871	Ribosomal protein S11 (RPS11)
152	125	101	0.822	0.664	Ribosomal protein S13 (RPS13)
147	84	1	0.571	0.007	Nicotinamide N-methyltransferase (NNMT)
147	180	35	1.224	0.238	Hemopexin (HPX)
146	89	121	0.610	0.829	Alpha-2-HS-glycoprotein (AHSG)

To avoid division by 0, a tag value of 1 for any tag that was not detectable was used.
NL, normal liver; NT, non-tumor; T, tumor.

More than 2 tags were detected in the intronic regions of the 164 genes in the NL, 168 genes in the NT, and 157 genes in the T library, suggesting that these regions might be potential intronic promoter regions (Table 4a). The biological process of these intron-origin transcripts using Human Protein Reference Database (http://www.hprd.org/) showed that these were related to basic cellular functions such as signal transduction, transport, and regulation of the nucleobase and nucleotide, suggesting that these intronic transcripts

Table 3a
Differentially expressed genes in HCC (top 10 from 5′SAGE).

5′SAGE T/NL	3′SAGE T/NL	5′/3′ Ratio	Gene
Up-regulated gene			
19	6	3.17	P antigen family, member 2 (prostate associated) (PAGE2)
18	10	1.8	Lectin, galactoside-binding, soluble, 4 (LGALS4)
16	3	5.33	Choline phosphotransferase 1 (CHPT1)
14	2	7	X antien family, member 1A (XAGE1A)
14	2	7	Dehydrogenase/reductase (SDR family) member 4 (DHRS4)
14	2	7	Sterol-C5-desaturase-like (SC5DL)
13	0.5	26	Coagulation factor XIII, B polypeptide (F13B)
13	2.33	5.58	Retinol dehydrogenase 11 (all-trans and 9-cis) (RDH11)
13	0.5	26	Transmembrane protein 14A (TMEM14A)
12	1.33	9.02	Dual specificity phosphatase 23 (DUSP23)
Down-regulated gene			
0.00436	0.0137	0.318	Hepcidin antimicrobial peptide (HAMP)
0.0051	ND		Metallothionein 1G (MT1G)
0.0068	0.04	0.17	Nicotinamide N-methyltransferase (NNMT)
0.00727	ND		Metallothionein 1E (functional) (MT1E)
0.0098	0.0526	0.186	C-reactive protein, pentraxin-related (CRP)
0.0145	ND		Metallothionein 1 M (MT1M)
0.0152	ND		Phospholipase A2, group IIA (platelets, synovial fluid) (PLA2G2A)
0.0178	0.111	0.16	Cytochrome P450, family 2, subfamily E, polypeptide 1 (CYP2E1)
0.0185	0.192	0.096	Metallothionein 2A (MT2A)
0.0201	ND		Metallothionein 1X (MT1X)

3′SAGE, 3′-end serial analysis of gene expression; 5′SAGE, 5′-end serial analysis of gene expression; HCC, hepatocellular carcinoma; NL, normal liver; T, tumor.

may play a fundamental role in the liver (data not shown). Among these genes, 12 were differentially expressed between the NL and T libraries more than four-fold (Table 4b). Interestingly, intronic transcripts (determined by 5′SAGE) of genes encoding *SAMD3*,

Table 3b
Differentially expressed genes in HCC (top 10 from 3′SAGE).

5′SAGE T/NL	3′SAGE T/NL	5′/3′ Ratio	Gene
Up-regulated gene			
ND	15		Leukocyte immunoglobulin-like receptor, subfamily B, member 1 (LILRB1)
ND	12		Fibroblast growth factor 5 (FGF5)
1	11	0.909	Adenosine deaminase, tRNA-specific 1 (ADAT1)
5	11	0.454	px19-like protein (PRELID1)
4.4	11	0.4	Anaphase promoting complex subunit 11 (ANAPC11)
ND	10.3		Chromosome 21 open reading frame 77 (C21orf77)
ND	10		von Willebrand factor (VWF)
2.333	10	0.233	ATX1 antioxidant protein 1 homolog (yeast) (ATOX1)
18	10	1.8	Lectin, galactoside-binding, soluble, 4 (LGALS4)
ND	9.5		Solute carrier family 26 (sulfate transporter), member 2 (SLC26A2)
Down-regulated gene			
0.5	0.012	41.7	ELL associated factor 1 (EAF1)
0.5	0.0137	36.5	TGF beta-inducible nuclear protein 1 (NSA2)
0.000436	0.0137	0.032	Hepcidin antimicrobial peptide (HAMP)
1	0.0179	55.9	Basic, immunoglobulin-like variable motif containing (BIVM)
ND	0.0182		DNA fragmentation factor, 45 kDa, alpha polypeptide (DFFA)
1	0.0185	54.1	GRIP1 associated protein 1 (GRIPAP1)
ND	0.0189		Nuclear factor of activated T-cells 5, tonicity-responsive (NFAT5)
1	0.0204	49	Adenylate cyclase 1 (ADCY1)
0.333	0.0312	10.7	Dihydroorotate dehydrogenase (DHODH)
0.738	0.0312	23.7	Ribosomal protein, large, P1 (RPLP1)

3′SAGE, 3′-end serial analysis of gene expression; 5′SAGE, 5′-end serial analysis of gene expression; HCC, hepatocellular carcinoma; NL, normal liver; T, tumor.

Please cite this article as: Y. Hodo, et al., Comprehensive gene expression analysis of 5′-end of mRNA identified novel intronic transcripts associated with hepatocellular carcinoma, Genomics (2010), doi:10.1016/j.ygeno.2010.01.004

Table 4a
Number of 5′SAGE tags mapped to intronic region.

	NL	NT	T
Tag mapped to intron	1287	1253	1292
Total promoter region	952	981	1020
(tag number = 1)	788	813	863
(tag number ≧2)	164	168	157

ACOX2, *HGD*, *CYP3A5*, *KNG1* and *AGXT* were increased, while their 3′ transcripts (determined by 3′SAGE) were decreased in HCC. In contrast, both 5′ intronic transcripts and 3′ transcripts encoding *HFM1*, *SERPINA1*, *SUPT3H*, *A2M* and *TMEM176B* were similarly decreased in HCC. Taken together, these data imply that the canonical- and intronic-promoter activities of a subset of genes including *SAMD3*, *ACOX2*, *HGD*, *CYP3A5*, *KNG1* and *AGXT* might be differently regulated in HCC.

ACOX2 as a novel intronic gene deregulated in HCC

A subset of genes listed above may be transcribed from intronic regions specifically in HCC. Among these genes, we focused on the regulation of *ACOX2*, which is reported to be potentially involved in peroxisomal beta-oxidation and hepatocarcinogenesis [20]. The intron-origin expression of *ACOX2* increased six-fold in HCC compared with the NT by 5′SAGE, while the expression based on the 3′end was almost similar between HCC and NT lesions (Table 4b). Close examination of 5′SAGE data identified two potential intron-origin transcripts of *ACOX2* (Supplemental Fig. 4). The first (intronic-*ACOX2-1*) was initiated upstream of the tenth exon, whereas the second (intronic-*ACOX2-2*) was initiated upstream of the twelfth exon of *ACOX2* (Supplemental Fig. 4). The sequence of the intronic part was unique, and the remaining part of the sequence was shared with the canonical transcripts of *ACOX2*.

The expression of canonical *ACOX2* and the two types of intron-origin transcripts was investigated in NL, NT, and T tissues by RT-PCR (Fig. 1A). Although canonical *ACOX2* expression was decreased in T than in NL, the intron-origin transcript, particularly intronic-*ACOX2-1*, was increased in T. Intronic-*ACOX2-2* transcripts also showed a modest increase. We further evaluated the alteration of these transcripts in 19 HBV-HCCs, 20 HCV-HCCs, and 4 non-B, non-C HCCs, and their background liver tissues by canonical *ACOX2* and intronic-*ACOX2* specific real-time detection (RTD)-PCR. Although the expression of canonical *ACOX2* was decreased, the expression of intronic-*ACOX2* was significantly increased (Fig. 1B). Importantly, the gene expression ratios of intronic-to canonical *ACOX2* increased more in moderately differentiated HCCs (mHCC) than in well-differentiated HCCs (wHCC), suggesting the involvement of intronic-*ACOX2* expression on HCC progression.

Table 4b
Differentially expressed intronic promoter regions in HCC.

5′SAGE T/NL	3′SAGE T/NL	5′/3′ Ratio	Gene
Up-regulated			
9	1	9.00	Sterile alpha motif domain containing 3 (SAMD3)
6	0.89	6.74	Acyl-Coenzyme A oxidase 2, branched chain (ACOX2)
6	0.62	9.68	Homogentisate 1,2-dioxygenase (homogentisate oxidase) (HGD)
6	0.009	666.67	Cytochrome P450, family 3, subfamily A, polypeptide 5 (CYP3A5)
5	0.64	7.81	Kininogen 1 (KNG1)
4	0.36	11.11	Alanine-glyoxylate aminotransferase (AGXT)
4	1	4.00	Crystallin, alpha A (CRYAA)
Down-regulated			
0.13	1	0.13	HFM1, ATP-dependent DNA helicase homolog (*S. cerevisiae*) (HFM1)
0.25	0.51	0.49	Serpin peptidase inhibitor, clade A member 1 (SERPINA1)
0.25	1	0.25	Suppressor of Ty 3 Homolog (*S. cerevisiae*) (SUPT3H)
0.25	0.2	1.25	Alpha-2-macroglobulin (A2M)
0.25	0.083	3.13	Transmembrane protein 176B (TMEM176B)

3′SAGE, 3′-end serial analysis of gene expression; 5′SAGE, 5′-end serial analysis of gene expression; HCC, hepatocellular carcinoma; NL, normal liver; NT, non-tumor; T, tumor.

Discussion

This is the first comprehensive transcriptional analysis of tissue lesions of non-B, non-C HCC, background liver and NL using the 5′ SAGE method. Approximately 6.7% of our 5′SAGE tags showed no matching within the human genome, possibly due to the presence of a single nucleotide polymorphism (SNP) in the human genome. Out of the complete matched tags in the genome, 70% were assigned to unique positions and 30% to two or more loci. The tags with multiple matches with genomic loci were largely retrotransposon elements, repetitive sequences, and pseudogenes.

In this study, the analysis of non-B, non-C HCC enabled us to evaluate direct molecular changes associated with HCC without any bias of gene induction by virus infection. The gene expression profile based on our 5′SAGE tags revealed that *albumin (ALB)* and apolipoproteins were highly expressed in NL, indicating the massive production of plasma proteins in NL; these results are similar to those of our previous study using 3′SAGE [6]. Other genes such as *aldolase B (ALDOB)*, *antitrypsin (SERPINA1)*, and *haptoglobin (HP)* were also highly expressed in NL, in both the 5′SAGE and 3′SAGE libraries (Table 2) [6]. Comparison of the expression profiles among NL, background NT and T identified several differentially expressed transcripts in T. *Galectin-4 (LGALS4)* was up-regulated and *HAMP*, *NNMT*, *CYP2E1*, and *metallothionein* were down-regulated in HCC in accordance with previous findings (Table 3a) [8,9,21]. Moreover, *CLEC4G*, which was predominantly expressed in the sinusoidal endothelial cells of the liver, was down-regulated in HCC. In addition, we first found that *P antigen family, member 2 (PAGE2)* and *XAGE1A* were up-regulated in HCC (Table 3a, Supplemental Fig. 1). These genes were members of cancer-testis antigen that include MAGE-family genes. MAGE-family members were originally found to be up-regulated in HCV-related HCC, and reported to be useful as molecular markers and as possible target molecules for immunotherapy in human HCC [22]. In this study, we identified that these members of genes were also up-regulated in non B, non-C HCC. Thus, these genes may be useful as molecular markers and therapeutic targets for the treatment of a certain type of human HCC.

There existed some discrepancy between 5′SAGE and 3′SAGE results, even though they were derived from the same sample. Technical issues such as amplication error, difference of restriction enzyme, and annotation error have been described previously [14]. It is possible that 3′ transcripts might be more stable than 5′ transcripts by binding of ribosomal proteins during translation. Another possibility is the diversity of the transcriptional start and/or termination sites. One of the advantages of 5′SAGE analysis is the potential to determine the transcriptional start sites in each gene. Indeed, a recent study indicated the importance of an insulin splice variant in the pathogenesis of insulinomas [23]. Considering the diversity of 5′ends of genes, it is more appropriate to perform 5′SAGE in combination with 3′SAGE when determining the frequency of gene expression and identifying novel transcript variants.

Here, we were able to identify at least 12 intron-origin transcripts that were differentially expressed in HCC compared with the background liver or NL. These transcripts could not be identified by the 3′SAGE approach. We also performed detailed expression analysis of *ACOX2* that was involved in the beta-oxidation of peroxisome. We

Please cite this article as: Y. Hodo, et al., Comprehensive gene expression analysis of 5′-end of mRNA identified novel intronic transcripts associated with hepatocellular carcinoma, Genomics (2010), doi:10.1016/j.ygeno.2010.01.004